Supporting information for

Bio-inspired copper complexes with Cu_2S cores: (Solvent)Effects on Oxygen Reduction Reactions.

Jordan Mangue,[a] Iris Wehrung,[b] Jacques Pécaut,[c] Stéphane Ménage,[a] Maylis Orio*[b] and Stéphane Torelli*[a]

[a] Univ. Grenoble Alpes, CNRS, CEA, IRIG, Laboratoire de Chimie et Biologie des Métaux, 17 rue des Martyrs, 38054 Grenoble Cedex 9, France.

[b] Aix Marseille Univ. Centrale Med, ISM2, Marseille, France.

[c] Univ. Grenoble Alpes, CEA, CNRS, IRIG, SYMMES, UMR 5819, F-38000 Grenoble, France.

Correspondence should be addressed to stephane.torelli@cea.fr or maylis.orio@univ-amu.fr

Table of Contents

Figure S4. Singly occupied molecular orbital (SOMO, left) and spin density plot (right) of **6** (DFT-optimized structure).

Figure S5. Difference electron density sketches of the main TD-DFT calculated absorptions of **6** (DFT-optimized structure).

Figure S6. Solid-state (black) and TD-DFT calculated (red) UV-Vis/NIR spectra of **6** (X-ray crystal structure).

Figure S7. Comparison between the CV curves recorded from the open-circuit potential toward the cathodic (A) and anodic (B) directions for **6** in acetone.

Figure S8. Stack plots of UV-Vis changes for the catalytic ORR by **1** in air-saturated acetone (**A**) and **6** in air-saturated acetone (**B**) and MeCN (**C**) at 298 K by monitoring the absorbance values at 750 nm corresponding to the accumulation of Me_8Fc^+.

Figure S9. Typical UV-vis changes for the catalytic ORR by **1** (1 molar eq.) with $LutHBF_4$ (400 molar eq.) and Me_8Fc (10, 20, 40, 60 80 and 100 molar eq.) in air-saturated acetone.

Figure S10. Kinetic profiles (Abs_{max}^{750nm}) for the catalytic ORR by **1** (1 molar eq.) / $LutHBF_4$ (400 molar eq.) / Me_8Fc (10, 20, 40, 60 80 and 100 molar eq.) in air-saturated acetone.

Figure S11. Typical UV-vis changes for the catalytic ORR by **6** (1 molar eq.) with $LutHBF_4$ (400 molar eq.) and Me_8Fc (10, 20, 40, 60 80 and 100 molar eq.) in air-saturated acetone.

Figure S12. Kinetic profiles (Abs_{max}^{750nm}) for the catalytic ORR by **6** (1 molar eq.) / $LutHBF_4$ (400 molar eq.) / Me_8Fc (10, 20, 40, 60 80 and 100 molar eq.) in air-saturated acetone.

Figure S13. Typical UV-vis changes for the catalytic ORR by **6** (1 molar eq.) with $LutHBF_4$ (400 molar eq.) and Me_8Fc (10, 20, 40, 60 80 and 100 molar eq.) in air-saturated MeCN.

Figure S14. Kinetic profiles (Abs_{max}^{750nm}) for the catalytic ORR by **6** (1 molar eq.) / $LutHBF_4$ (400 molar eq.) / Me_8Fc (10, 20, 40, 60 80 and 100 molar eq.) in air-saturated MeCN.

Figure S15. H_2O_2 calibration curve using the TiO-tpyp reagent and corresponding UV-vis traces.

Figure S16. Comparison of the CV curves recorded from the open-circuit potential toward the cathodic (A) and anodic (B) directions for **6** in MeCN.

Figure S17. CVs of **6** (0.7 mM) in acetone at different scan rates and experimental plot of Ψ *vs* $v^{-1/2}$ for the redox $Cu^{II}Cu^{I}/Cu^{II}Cu^{II}$ process in **6**.

Figure S18. CVs of **6** (0.6 mM) in MeCN at different scan rates and experimental plot of Ψ *vs* $v^{-1/2}$ for the redox $Cu^{II}Cu^{I}/Cu^{II}Cu^{II}$ process in **6**.

Table S1. Crystal data and structure refinement for **6**.

Table S2. Bond length [Å] for **6**.

Table S3. Bond angles [deg] for **6**

Table S4. NBO analysis of the Cu-Cu bond in mixed-valent Cu^{II}-Cu^{I} species: Comparison of the results obtained for DFT-optimized and X-ray crystal structures of **6** featuring different metal-metal bond lengths.

Table S5. Mulliken spin population analysis for **6** (DFT-optimized structure).

Table S6. Computed *g*-values and copper hyperfine coupling constants for **6** (DFT-optimized structure).

Table S7. Theoretical assignments of the main bands of the UV-Vis/NIR spectrum of **6** based on the DFT-optimized structure.

Table S8. Theoretical assignments of the main bands of the UV-Vis/NIR spectrum of **6** based on the X-ray crystal structure.

Table S9. Calculated redox potentials for the $Fc^{+/0}$ couple.

Table S10. Calculated redox potential for the Cu(II)Cu(I)/Cu(I)Cu(I) couple of **6** (DFT-optimized structure).

Table S11. ORR experiments performed with **1** and **6** in acetone or MeCN at room temperature using Me_8Fc and $LutHBF_4$ as electron and proton sources.

Table S12. Crystal data and structure refinement for **II**.

Table S13. Bond length [Å] for **II**.

Table S14. Bond angles [deg] for **II**

Cartesian coordinates from DFT calculations

Experimental section

All chemicals are from Acros Organics, Merck, or Lancaster. Acroseal® purity solvents were used for air-sensitive experiments. Complex **1** was prepared according to our reported procedure.[1] LutHBF$_4$, Me$_8$Fc, Me$_2$Fc$^+$, Me$_8$Fc$^+$ and Me$_{10}$Fc$^+$ were prepared according to reported procedures.[2-4] Air-sensitive materials were manipulated in an Argon flushed glove box (O_2 and H_2O < 2 ppm). **Electrospray ionization mass spectrometry** (ESI-MS) **spectra** were recorded with a Bruker Daltonics Esquire 3000 Plus device. **X-ray crystallography** data were acquired at 150 K using an Oxford-diffraction XCalibur S diffractometer with graphite monochromated MoKα radiation (λ = 0.71073 Å). Molecular structure was solved by direct methods and refined on F^2 by full matrix least squares techniques using SHELX TL package. All non-hydrogen atoms were refined anisotropically, and hydrogen atoms were placed in ideal positions and refined as riding atoms with individual isotropic displacement parameters. **X-band EPR** spectra were obtained on a Bruker EMX spectrometer equipped with an Oxford ESR 910 cryostat for low temperature studies. The microwave frequency was calibrated with a frequency counter and the magnetic field with an NMR gaussmeter. Spectra were analyzed with the WIN-EPR software and numerical simulation was conducted using the Matlab toolbox EasySpin 5.2.3.[5] **Electrochemical experiments** were performed in an argon-flushed glove box. A three-electrode setup was used, and consists of a glassy carbon (3mm in diameter) disk as a working electrode, a platinum wire serves as auxiliary electrode and a leakless Ag/AgCl electrode (Model ET069 from EDAQ) as reference electrode directly dipped into the solution. Cyclic voltammograms were recorded with a Bio-logic SP-300 potentiostat piloted by the EC-Lab software. All measurements were externally referenced to ferrocene. **Solution UV-Vis/NIR** spectra were recorded on a Perkin Elmer Lambda 1050 Spectrophotometer operating at room temperature equipped with appropriate optic fibres and connected to a glovebox. Spectral adjustments were performed using the Origin software. **Solid-state UV-Vis/NIR** spectra were acquired on a Perkin Elmer Lambda 1050 Spectrophotometer

operating at room temperature equipped with a 150 nm integration sphere. **Kinetics** were recorded with a Lambda 465 (PerkinElmer) diode array spectrophotometer and **H_2O_2 concentrations** were determined according to the procedure described below using a Shimadzu 1800 device.

Evaluation of the electron self-exchange rate constants k_{el} and k_{hom}. The method of Nicholson[6] was used to determine the standard electrochemical electron self-exchange rate constant k_{el} (cm s^{-1}) for **6** ($Cu^{II}Cu^{I} \rightarrow Cu^{I}Cu^{I}$ monoelectronic reduction process). k_{el} can be obtained, under "quasi-reversible" conditions, from:

$$\Psi = k_{el}(D_R/D_O)^{\alpha/2}(RT/nF\pi D_R)^{1/2}/v^{1/2}$$

Where n is the number of electrons exchanged (1 in this case), *v* is the potential scan rate (V s -1), α is the transfer coefficient, and π, F, R, and T have their usual significance. D_R and D_O are the diffusion coefficients of the reduced and oxidized species in each solvent. D_R values of $7.7(2)\cdot10^{-6}$ cm^2s^{-1} and $7.1(3)\cdot10^{-6}\cdot cm^2\cdot s^{-1}$ where obtained in acetone and MeCN, respectively using the Randles-Sevcik equation:

$$i_p = 2.69\cdot10^5 \times n^{3/2} \times A \times C \times (D\cdot v)^{1/2} \text{ at } 25°C$$

where i_p is the current maximum in amps, n is the number of electrons transferred in the redox event (1 in our case), A is the electrode area in cm2, C in the concentration of the given complex, D is the diffusion coefficient of the complex in $cm^2\cdot s^{-1}$ and *v* is the scan rate in $V\cdot s^{-1}$.

Confirmation that $D_O \approx D_R$ was obtained in both solvents from the nearly identical values of i_{pa} and i_{pc}. $(D_R/D_O)^{\alpha/2}$ was consequently set to 1.

Cyclic voltammograms of **6** (0.7 mM in acetone + 0.1 M Bu_4NPF_6 and 0.6 mM in MeCN + .1 M Bu_4NPF_6) were recorded at different potential scan rates in the appropriate potential region (Figures S17 and S18). Under these conditions, an increase of ΔEp as a function of v was observed (from 130 to 180 mV in the 0.025 – 0.4 V $s^{-}1$ range in acetone and from 77 to 88 mV in the 0.05 – 0.4 V $s^{-}1$ range in MeCN). For each ΔEp value, Ψ can be calculated using the empirical equation:[7]

$$\Psi = (-0.6288+0.0021n\Delta Ep)/(1-0.017n\Delta Ep)$$

From all that, plotting Ψ *vs* $v^{-1/2}$ allows an estimate of k_{el} in both solvents (Figures S17 ad S18)

Then, the homogeneous electron self-exchange rate constant khom can be calculated as it is correlated with k_{el} as described by Weaver[8] by:

$$k_{hom} = 4\pi \times N_A \times rh^2 \times k_{el} 10^{-19}$$

where N_A is the Avogadro constant (mol-1) and rh is the internuclear distance for self-exchange (Å). The value of rh was set to 2r (14 Å), where r is the radius of **6**, approximated to a sphere from the X-ray crystal structure.

Computational details.

All theoretical calculations were based on the Density Functional Theory (DFT) and were performed with the ORCA program package.[9, 10] Full geometry optimizations were carried out using the BP86 functional[11, 12] in combination with the def2-TZVP basis sets[13] for all atoms. Increased integration grids (Grid2 in ORCA convention) and tight SCF convergence criteria were used. To resemble the experimental conditions as closely as possible, all calculations including geometry optimizations were performed in acetone solvent by invoking the Control of the Conductor-like Polarizable Continuum Model (CPCM).[14] To ensure that the resulting structures converged to a local minimum on the potential energy surface, frequency calculations were performed and resulted in only positive normal vibrations. The Gibbs free energies were computed from the optimized structures as a sum of electronic energy, solvation, and thermal corrections to the free energy. Redox potentials were obtained from the calculated free energy change between oxidized and reduced species in solution. They are relative potentials referenced to the ferrocene couple and, as such, a computed value of 4.893 V was subtracted to make direct comparisons to experimental data.[15] NBO analysis was performed using the Gaussian09 package[16] with inclusion of the 3-center bond option in the search algorithm.[17, 18] Electronic structures were obtained from single-point DFT calculations using the B3LYP functional[19, 20]

together with the def2-TZVP basis sets.[13] EPR parameters, namely *g*-tensors, were obtained from single-point calculations using a modified version of B3PW91[19, 21,] with 40% exact (Hartree–Fock) exchange.[22] The large aug-cc-pVTZ-Jmod basis set[23] was applied for the metal center while the def2-TZVP basis sets[13] were used for all other atoms. Hyperfine tensors were obtained from single-point calculations using the B3PW91 functional[19, 21] together with the aug-cc-pVTZ-Jmod basis set[23] for the metal center and the def2-TZVP basis sets[13] for all other atoms. UV-vis spectral features were predicted using TD-DFT using the CAM-B3LYP functional[19, 20, 24] and the def2-TZVP basis sets.[13] Vertical electronic transitions were calculated using time-dependent DFT within the Tamm-Dancoff approximation (TDA).[25-28] To increase computational efficiency, the RI approximation[29] was used in calculating the Coulomb term, and at least 70 excited states were calculated in each case. Spin density plots, molecular orbitals as well as difference density plots for each transition were generated using the orca plot utility program and were visualized with the Chemcraft program (http://chemcraftprog.com).

Determination of the extinction coefficients of Me_8Fc^+ in acetone. Electron-transfer oxidation of Me_8Fc in acetone with cerium(IV) ammonium nitrate (CAN) was performed in a UV cell at 298 K. A ε values of 460 $M^{-1}cm^{-1}$ at 750 nm for Me_8Fc^+ was determined with Beer's Law.

Catalytic H_2O_2 production, detection and quantification. The formation of Me_8Fc^+ in the presence of **1** or **6** and *2,6*-lutidinium tetrafluoroborate ($LutHBF_4$) was monitored in air-saturated acetone or MeCN at 298 K by visible absorption spectroscopy. In a typical experiment (1/40/400 Cat/Me_8Fc/LutH), an air-saturated solution of $LutHBF_4$ (25 µL, 2.0 M, 50 µmol, 400 molar eq.) was added to an air-saturated solution of Me_8Fc (2.225 mL, 2.24 mM, 4.98 µmol, 40 molar eq.) in a septum-sealed quartz cuvette (1 cm). An Ar-saturated solution of **1** or **6** (250 µL, 0.5mM, 0.125 µmol, 1 molar eq.) was then added. Kinetics traces at λ_{max}^{Me8Fc+} (λ_{max} = 785 nm, ε = 390 M^{-1} cm^{-1}

in MeCN and 460 M^{-1} cm^{-1} in acetone) were monitored using a Lambda 465 (PerkinElmer) diode array spectrophotometer. Control experiments were performed in an identical manner by adding 250 µL of MeCN or $[Cu(CH_3CN)_4]OTf$ at 1 mM (to take into account the dinuclearity of **1** and **6**). All the experiments were triplicated, yielding highly reproducible data (95% identity). The amount of hydrogen peroxide produced was determined by spectroscopic titration with an acidic solution of $TiO(tpypH_4)^{4+}$ complex (TiO-tpyp reagent).[30, 31] The TiO-tpyp reagent (~4.5. 10^{-5} M) was prepared by dissolving 3.45 mg of the [TiO(tpyp)] complex (≥90%, from TCI) in 100 mL of 0.05 M $HCl_{(aq)}$ and stored at 277 K. A small portion (15 µL) of each sample solution (collected after observing stable absorbance values along time) was added to a mixture of TiO-tpyp reagent (250 µL), 4.8 M perchloric acid (250 µL) and water (235 µL). The resulting solution was stirred for 5 min at 298 K. After dilution to 2.5 mL with distilled water, the solution was transferred in a quartz UV-vis cell (1 mm) and the absorbance at λ = 433 nm was read using a Shimadzu 1800 device. For the blank experiments, MeCN (15 µL) was used in place of the reaction mixture. All the experiments were triplicated (97% identity). The H_2O_2 content for sample (n) follows:

$\Delta Asample_{(n)}$ = Ablank – $Asample_{(n)}$, (n) being the sample number (eqn 1)

A calibration curve (Fig S14) was independently obtained using the same procedure (1 mm cuvette) and H_2O_2 solutions (prepared by cascade dilutions of commercial 30% H_2O_2 titrated at 9.8 M with the $KMnO_4$ method.[30] The obtained ΔA values ($\Delta Acal_{(n)}$) were plotted against H_2O_2 concentration in the final sample, $[H_2O_2]_{final\_sample}$(µM), giving the following calibration curve equation:

$[H_2O_2]$final sample =(ΔA+0.0065) / 0.01827 (eqn2)

Based on eqn. 2, the amount of hydrogen peroxide in the catalytic reactions was determined based on $\Delta Asample_{(n)}$. $[H_2O_2]$ in the reaction mixture was calculated considering the dilution factor:

$[H_2O_2]_{mother\_sample}(\mu M)=[H_2O_2]_{final\_sample}*(2500/15)$ (eqn3)

The results were then confronted to the theoretical $[H_2O_2]$ for a 100% yield and the remaining electron consumption finally attributed to H_2O production.

Preparation of [(benzylamino)methyl]pyridine.

Under inert atmosphere, benzaldehyde (981 mg, 9.25 mmol, 1 eq.) and 6-methylaminepyridine (1.00 g, 9.25 mmol, 1 eq.) were dissolved in EtOH (20 mL) and stirred for 1 h at room temperature. Solid $NaBH_4$ (700 mg, 18.5 mmol, 2 eq.) was then slowly added portion wise over 30 min. The mixture was stirred for an additional 30 min and then refluxed for 12 h. After cooling to room temperature, the solution was diluted with EtOH (5 mL) and carefully hydrolyzed with 4 M HCl (10 mL). 20 % aq. NaOH solution was then added until pH = 12. The medium was extracted with CH_2Cl_2 and dried over Na_2SO_4. After evaporation of the solvents, the title compound was obtained as a green/yellow oil (1.69 g, 93 %) and used without further purification.

^{1}H NMR (300 MHz, $CDCl_3$, δ ppm): 8.57 (d, 3J = 4.2 Hz, 1H), 7.65 (dt, 3J = 7.8 Hz, 4J = 1.8 Hz, 1H), 7.28 (m, 7H), 3.95 (s, 2H), 3.87 (s, 2H), 2.24 (broad, 1H).

^{13}C NMR (75 MHz, $CDCl_3$, δ ppm): 159.9, 149.4, 140.3, 136.5, 128.5, 128.3, 127.1, 122.4, 122.0, 54.6, 53.6.

ESI-MS: m/z = 199.3 $[M + H^+]^+$.

Preparation of II.

Under inert atmosphere, **I** (246 mg, 0.98 mmol, 1 eq.)[1] was suspended into a degassed NaOH solution (1 M, 75 mL). The reaction mixture was stirred for 3 h at 50°C. The resulting orange mixture was filtered while cannulated. After cooling at 0°C, 6 M HCl (15 mL) was added dropwise until the orange color disappeared and a white solid (free thiol) precipitated. The solid was filtered and dissolved in a minimum of CH_2Cl_2 (about 150 mL), dried over Na_2SO_4 and the solvent evaporated. The residue was then dissolved in THF (50 mL) and the solution degassed with argon. Et_3N (250 µl, 1.79 mmol, 1.8 eq.) was added under argon to give a bright orange solution (thiophenolate). Freshly prepared and degassed I_2 solution (0.05 M in THF) was then added dropwise until the orange color disappeared. Addition of few drops of Et_3N followed by I_2 solution (10 mL in total) was subsequently repeated until addition of Et_3N no longer affords the orange colored solution (reaction completion). THF was evaporated, the residue extracted with CH_2Cl_2/H_2O and the combined organic layers dried over Na_2SO_4. After evaporation, the residue was filtered over a short SiO_2 column using CH_2Cl_2 as eluent. **II** was recovered as a yellow solid (120 mg, 70 %) and used without further purification. X-ray quality crystal were obtained by slow

evaporation of a CH_2Cl_2 solution of **II** (CCDC deposition number 2347077, Tables S12-S14 for details)

^{1}H NMR (300 MHz, $CDCl_3$, δ ppm): 10.24 (s, 4H), 7.93 (s, 4H), 2.51 (s, 6H).

^{13}C NMR (75 MHz, $CDCl_3$, δ ppm): 189.3, 143.1, 138.2, 136.4, 134.9, 21.4.

ESI-MS: m/z = 381.0 $[M + Na+]^+$.

Anal. calcd for $C_{18}H_{14}O_4S_2$•0.5 CH_2Cl_2: C, 55.43%; H, 3.77%. Found: C, 55.21%; H, 3.85%.

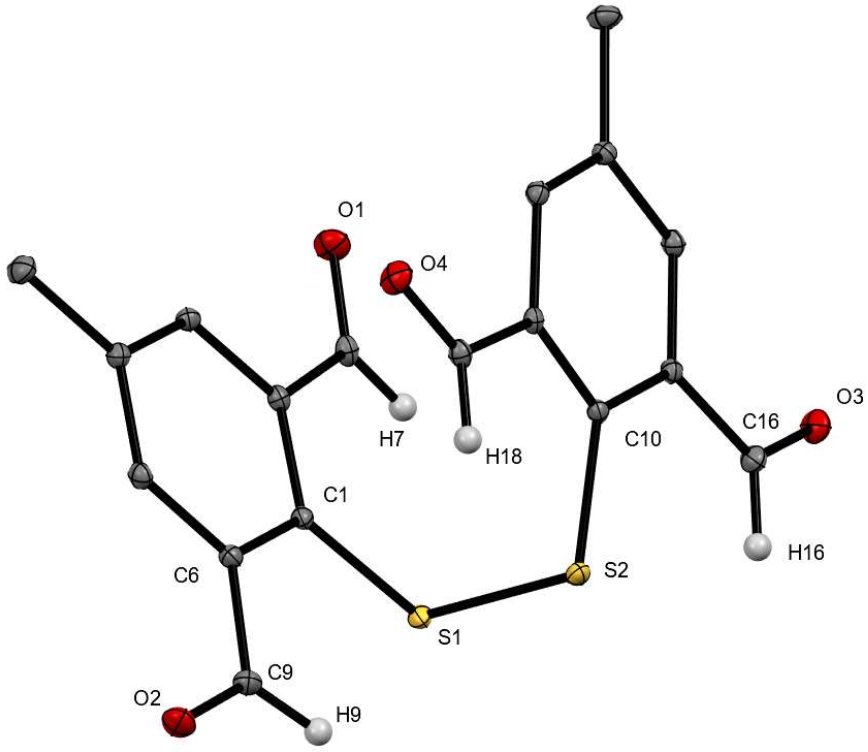

ORTEP diagram (30 % probability) for **II**. Non-representative hydrogen atoms are omitted for clarity; see Tables S12-S14 for full details.

Preparation of (BAMP)$_2^{S\text{-}S}$.

Under inert atmosphere, Na_2SO_4 (2 g) and glacial acetic acid (77 µL, 1.34 mmol, 3.2 eq.) were added to a solution of **II** (150 mg, 0.42 mmol, 1 eq.) in $(ClCH_2)_2$ (8 mL). A solution of [(benzylamino)methyl]pyridine (410 mg, 2.09 mmol, 5 eq.) in 7 mL of $(ClCH_2)_2$ was added dropwise and the mixture stirred for 15 min. $Na[HB(OAc)_3]$ (541 mg, 2.51 mmol, 6 eq.) was then introduced portion wise within 30 min and the reaction stirred at room temperature for 48 h. After filtration

and evaporation, the crude oil was dissolved in a biphasic Et_2O/H_2O solution (15 mL/15 mL) and extracted with Et_2O (2*15 mL). The combined organic layers were washed with water, $NaHCO_{3(sat)}$ and dried over Na_2SO_4. After evaporation, the crude oil was purified by column chromatography (SiO_2, Et_2O 100 % → AcOEt 100%). **$(BAMP)_2^{S\text{-}S}$** was obtained as a yellowish oil (100 mg, 43 %).

^{1}H NMR (300 MHz, $CDCl_3$, δ ppm): 8.42 (d, ^{3}J = 3.9 Hz, 4H), 7.48 (dt, ^3J = 7.8 Hz, ^4J = 1.8 Hz, 4H), 7.40 (s, 2H), 7.37 (s, 2H), 7.29 (s, 4H), 7.23 (m, 14H), 7.16 (m, 4H), 7.00 (dt, ^3J = 6.0 Hz, ^4J = 1.2 Hz, 4H), 3.53 (s, 14H), 3.39 (s, 8H) 2.30 (s, 6H).

^{13}C NMR (75 MHz, $CDCl_3$, δ ppm): 160.2, 148.8, 143.8, 139.4, 139.1, 136.2, 132.4, 129.0, 128.9, 128.2, 126.9, 122.6, 121.7, 59.7, 58.6, 56.8, 21.8.

ESI-MS: m/z = 1087.0 $[M + H^+]^+$.

Anal. Calcd for $C_{70}H_{70}N_8S_2$•0.2 AcOEt: C, 76.95; H, 6.53; N, 10.14. Found: C, 76.57; H, 6.47; N, 10.29.

Preparation of 6.

In the glove box, a solution of $[Cu(CH_3CN)_4]OTf$ (73.0 mg, 0.19 mmol, 4.1 eq) in acetone (2 mL) was added to a solution of the ligand (50 mg, 0.046 mmol, 1 eq.) in acetone (1.5 mL). The reaction mixture immediately turned violet. After 5 min stirring, the solution was filtered over millipore and half of the solvent evaporated. Slow addition of diethyl ether induced precipitation of **6** that was collected by filtration as a dark colored powder. X-ray quality crystals were obtained by layering pentane onto a concentrated acetone solution of the complex. The CCDC deposition number for **6** is 2347081.

Anal. Calcd for $C_{70}H_{70}N_8S_2$•0.1 Et_2O: C, 46.01; H, 3.72; N, 5.74. Found: , 45.79; H, 3.91; N, 5.98.

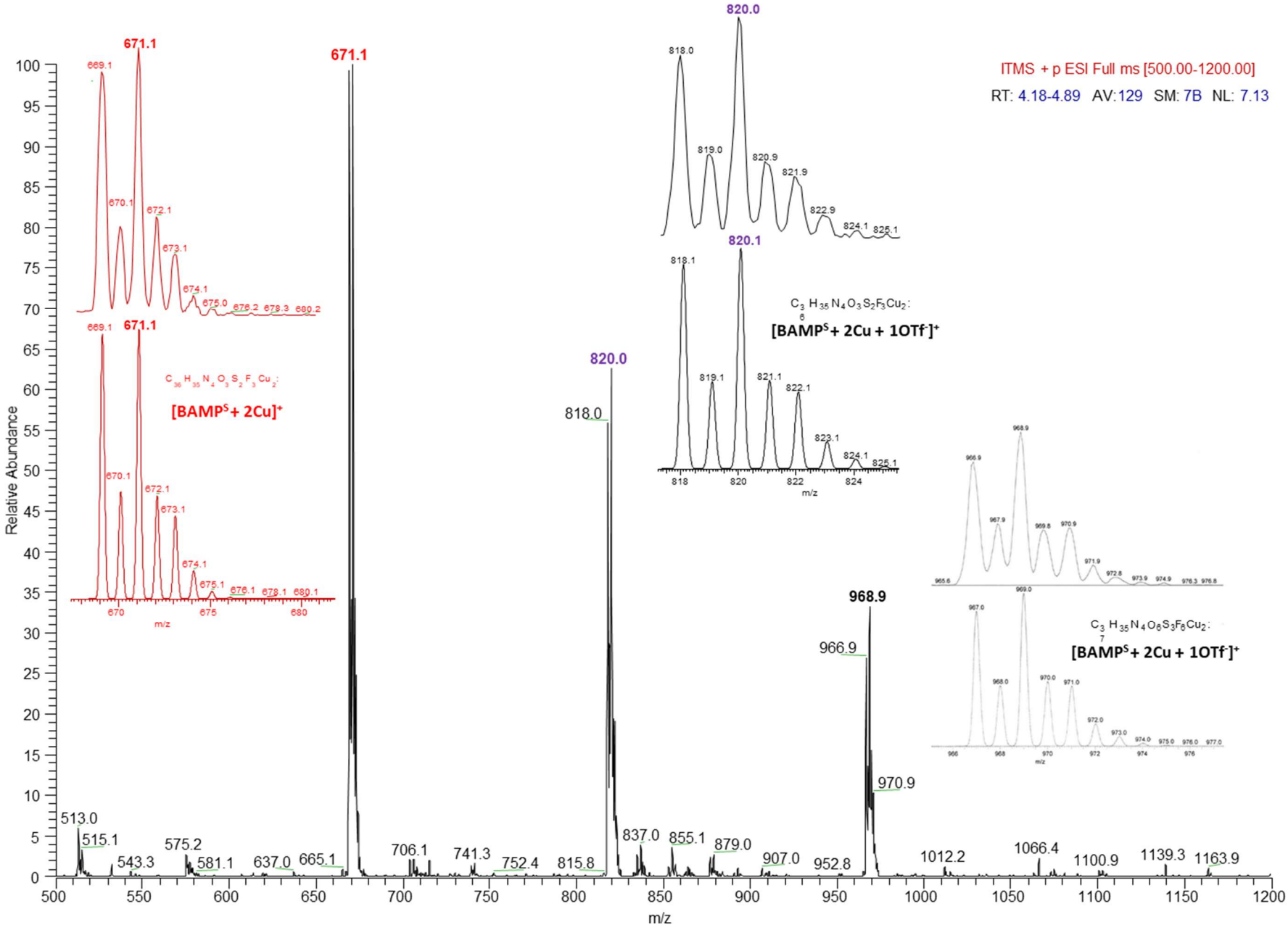

Figure S1. ESI spectrum of **6** in acetone.

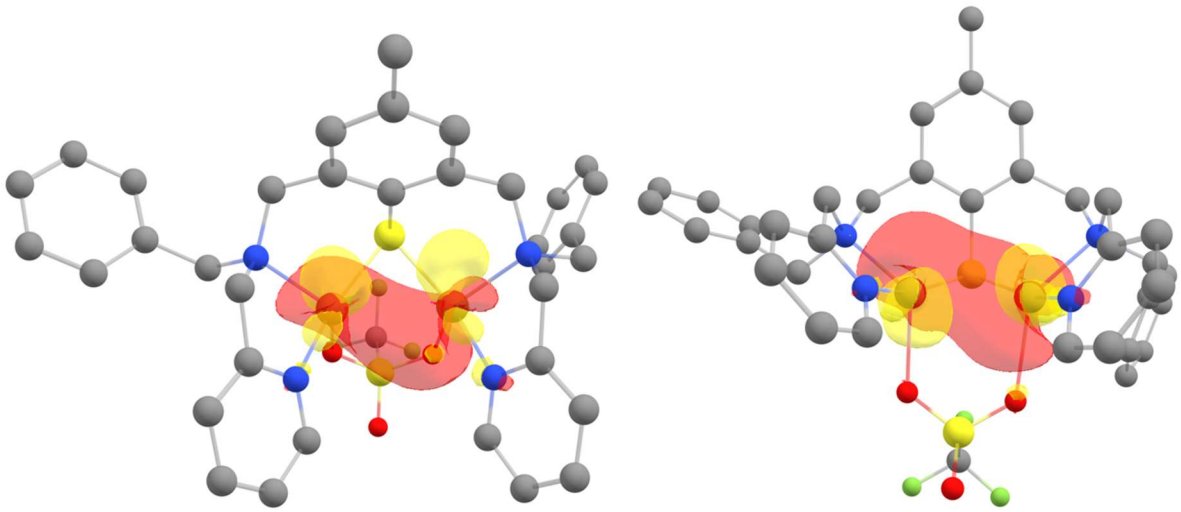

Figure S2. Selected views for the occupied natural orbital relevant to the Cu–Cu bond in DFT-optimized structure of **6**. Color scheme: Cu brown, S yellow, O red, N dark blue, F green and C light grey. Hydrogen atoms are omitted for clarity.

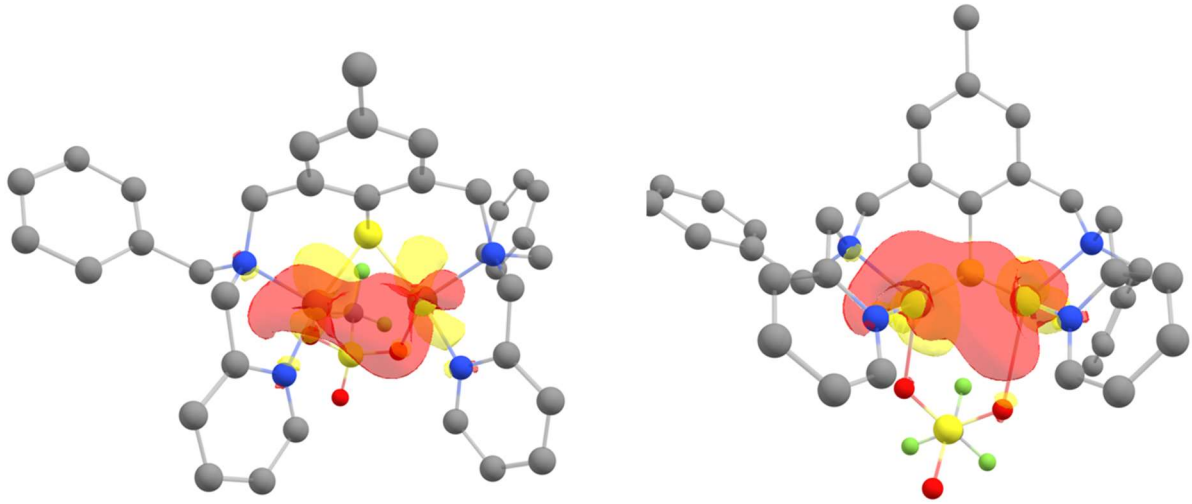

Figure S3. Selected views for the occupied natural orbital relevant to the Cu–Cu bond of **6** (X-ray crystal structure). Color scheme: Cu brown, S yellow, O red, N dark blue, F green and C light grey. Hydrogen atoms are omitted for clarity.

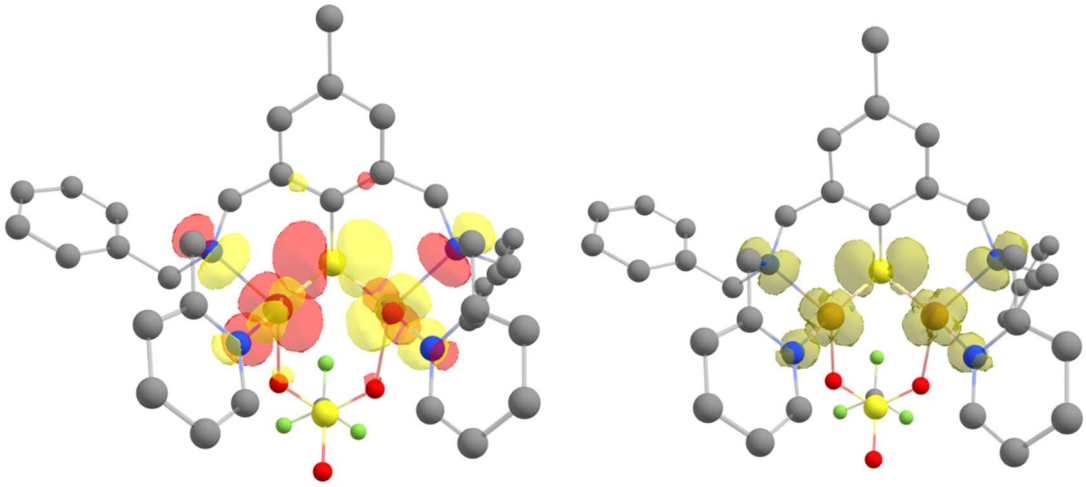

Figure S4. Singly occupied molecular orbital (SOMO, left) and spin density plot (right) of **6** (DFT-optimized structure). Color scheme: Cu brown, S yellow, O red, N dark blue, F green and C light grey. Hydrogen atoms are omitted for clarity.

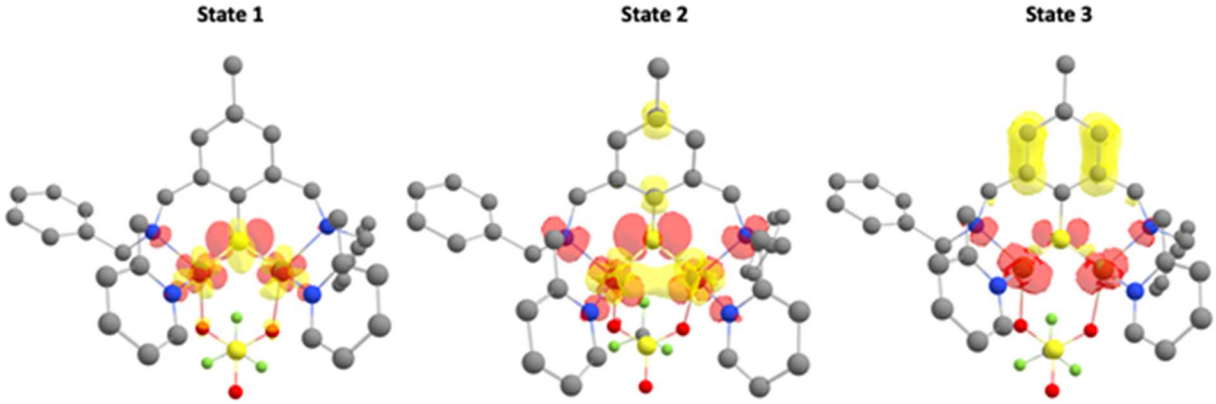

Figure S5. Difference electron density sketches of the main TD-DFT calculated absorptions of **6** (DFT-optimized structure). Yellow = negative density, donor state; red = positive density, acceptor state. Color scheme: Cu brown, S yellow, O red, N dark blue, F green and C light grey. Hydrogen atoms are omitted for clarity.

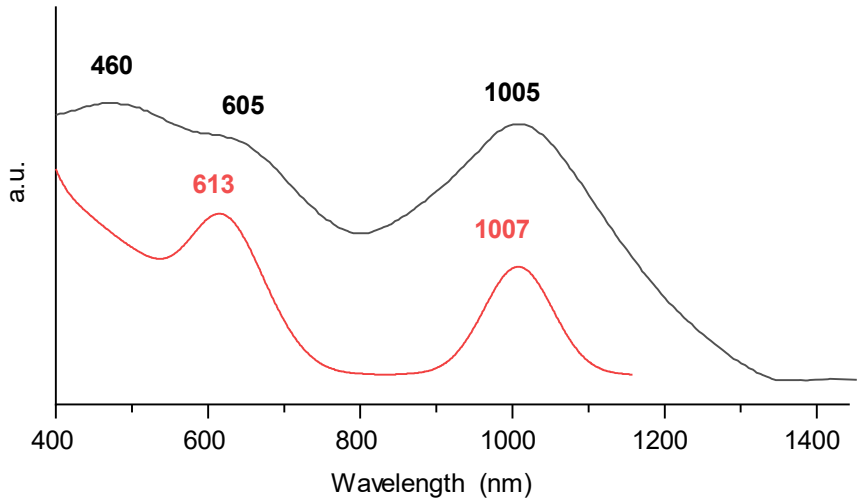

Figure S6. Solid-sate (black) and TD-DFT-calculated (red) UV-Vis/NIR spectrum of **6** (X-ray crystal structure).

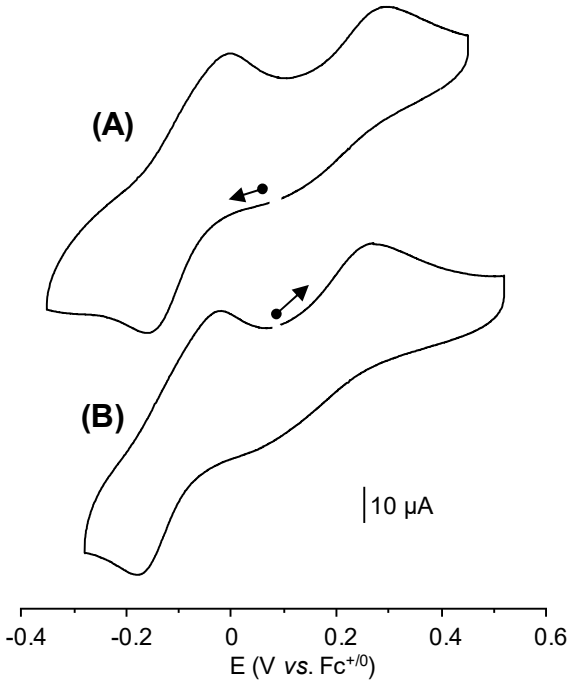

Figure S7. Comparison between the CV curves recorded from the open-circuit potential toward the cathodic (A) and anodic (B) directions. Conditions **6** at 0.7 mM in acetone + 0.1 M $TBAPF_6$ as supporting electrolyte and glassy carbon as working electrode. The curves corresponds to the initial scan at 100 $mV.s^{-1}$.

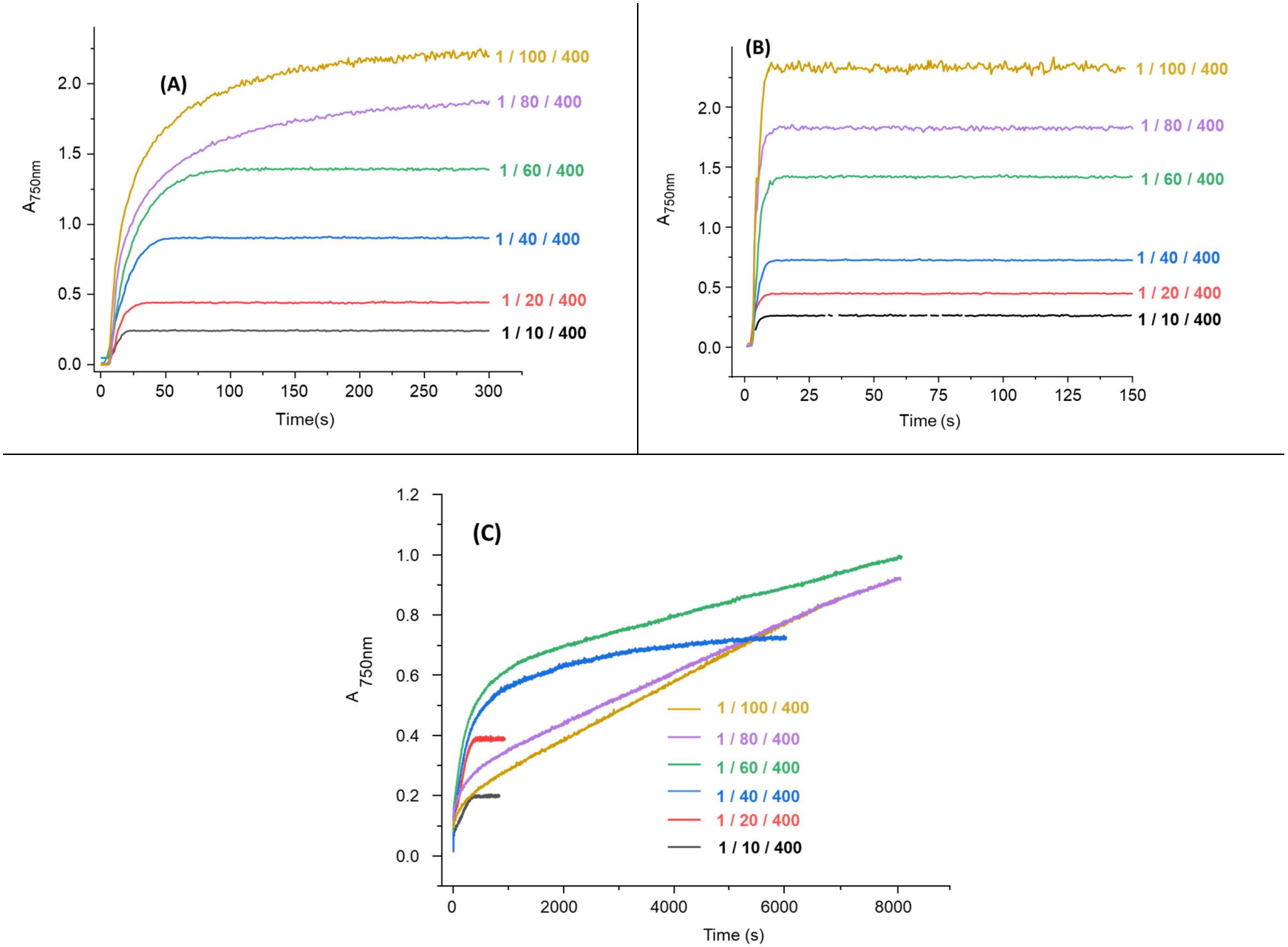

Figure S8. Stack plots of UV-Vis changes for the catalytic ORR by **1** in air-saturated acetone **(A)** and **6** in air-saturated acetone **(B)** and MeCN **(C)** at 298 K by monitoring the absorbance values at 750 nm corresponding to the accumulation of Me_8Fc^+.

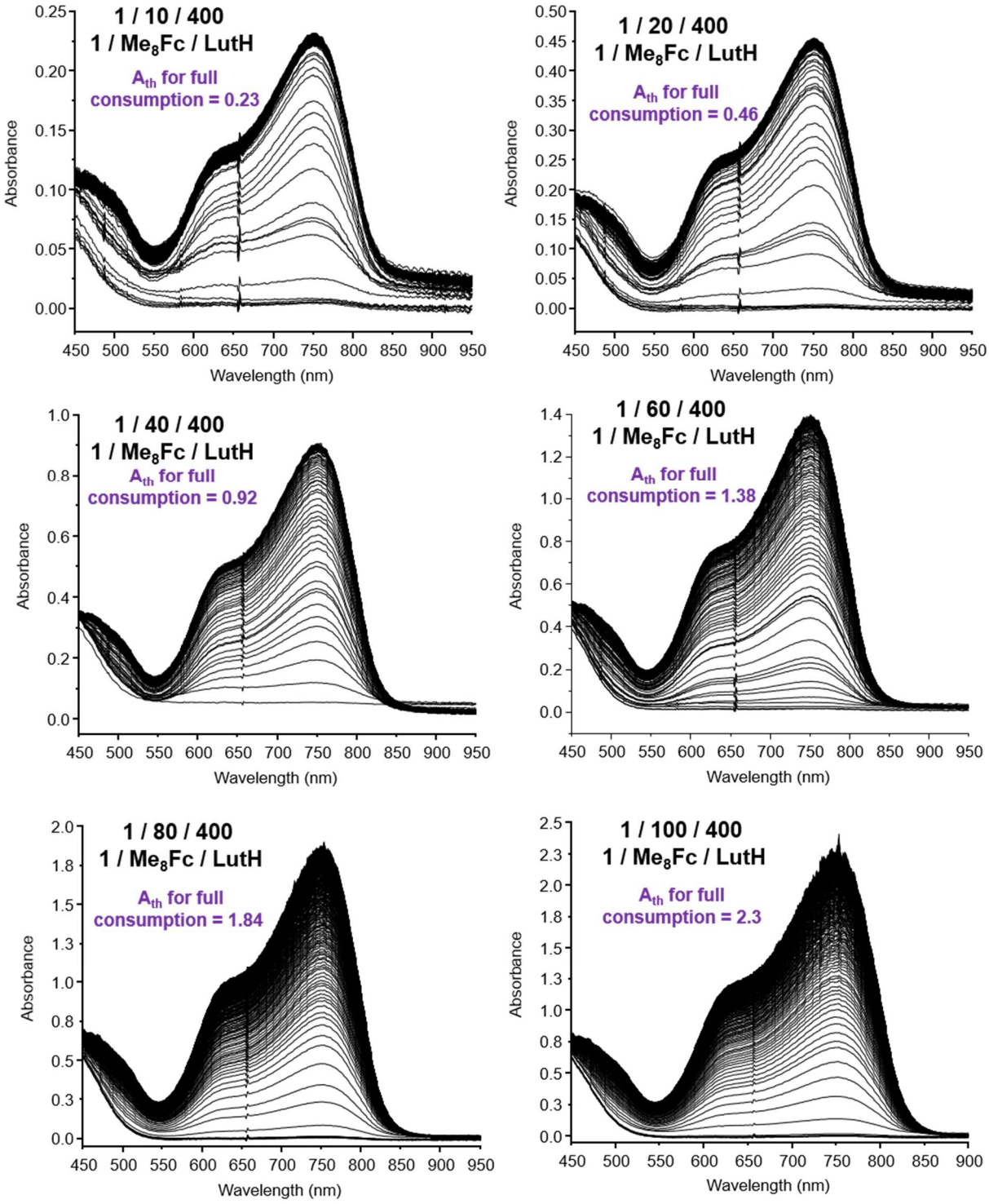

Figure S9. Typical UV-vis changes for the catalytic ORR by **1** (1 molar eq.) / $LutHBF_4$ (400 molar eq.) / Me_8Fc (10, 20, 40, 60, 80 and 100 molar eq.) in air-saturated acetone. For each dataset, the theoretical absorbance value corresponding for full Me_8Fc consumption is indicated.

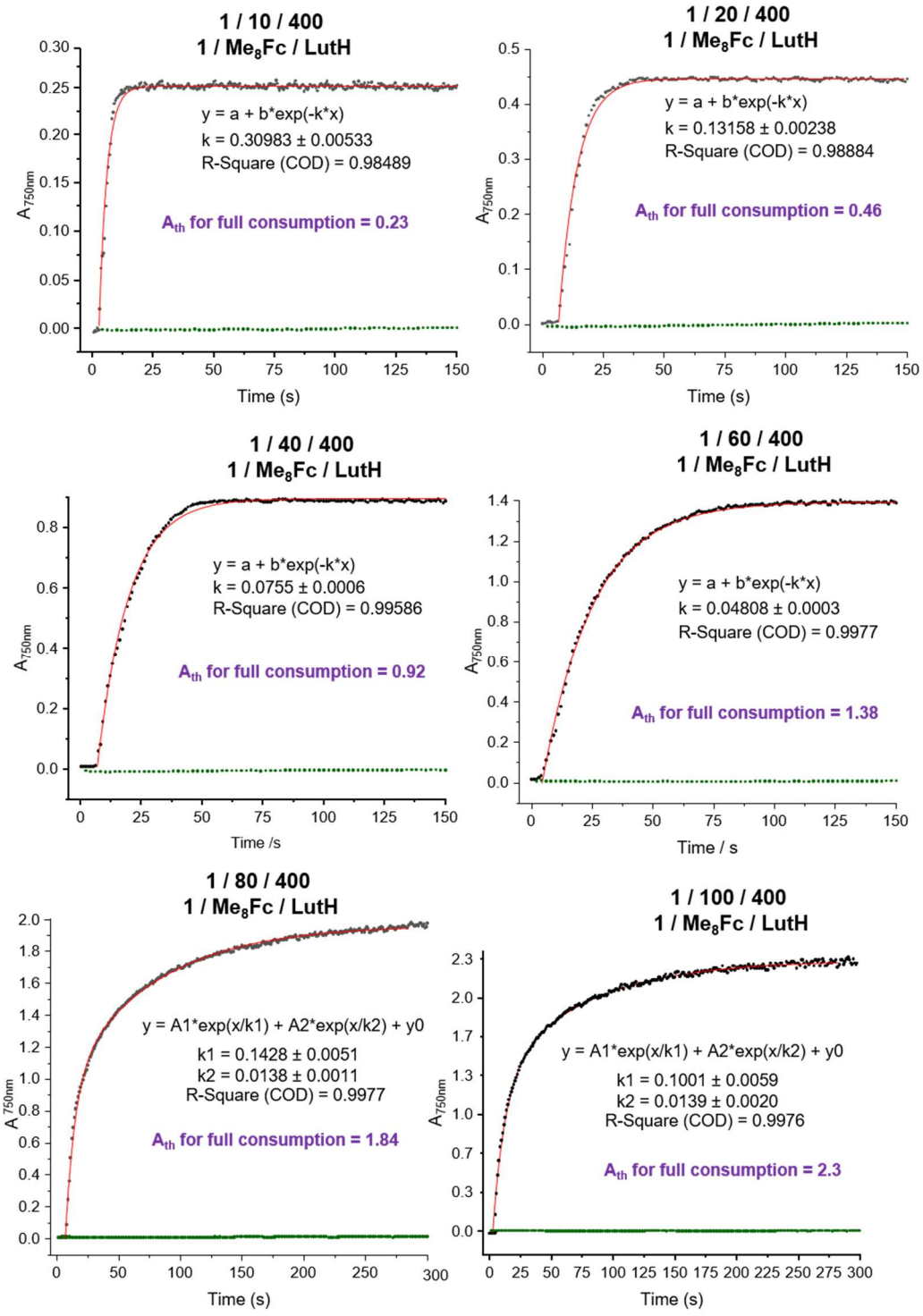

Figure S10. Kinetic profiles (Abs_{max}^{750nm}) for the catalytic ORR by **1** (1 molar eq.) / $LutHBF_4$ (400 molar eq.) / Me_8Fc (10, 20, 40, 60, 80 and 100 molar eq.) in air-saturated acetone together with the blank experiments (green dots) performed with commercial $[Cu(CH_3CN)_4](OTf)$. For each dataset, the theoretical absorbance value corresponding for full Me_8Fc consumption is indicated.

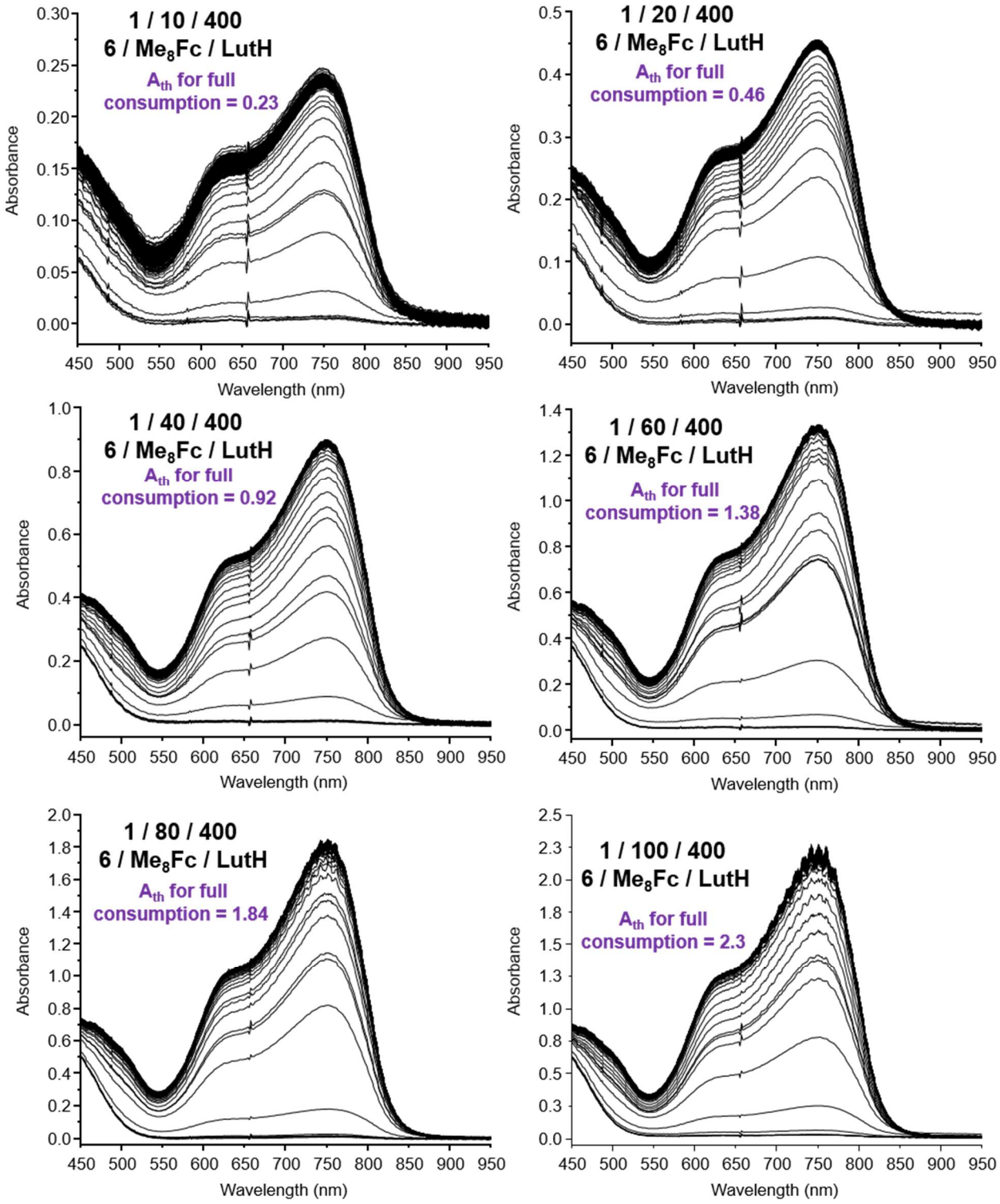

Figure S11. Typical UV-vis changes for the catalytic ORR by **6** (1 molar eq.) / $LutHBF_4$ (400 molar eq.) / Me_8Fc (10, 20, 40, 60, 80 and 100 molar eq.) in air-saturated acetone. For each dataset, the theoretical absorbance value corresponding for full Me_8Fc consumption is indicated.

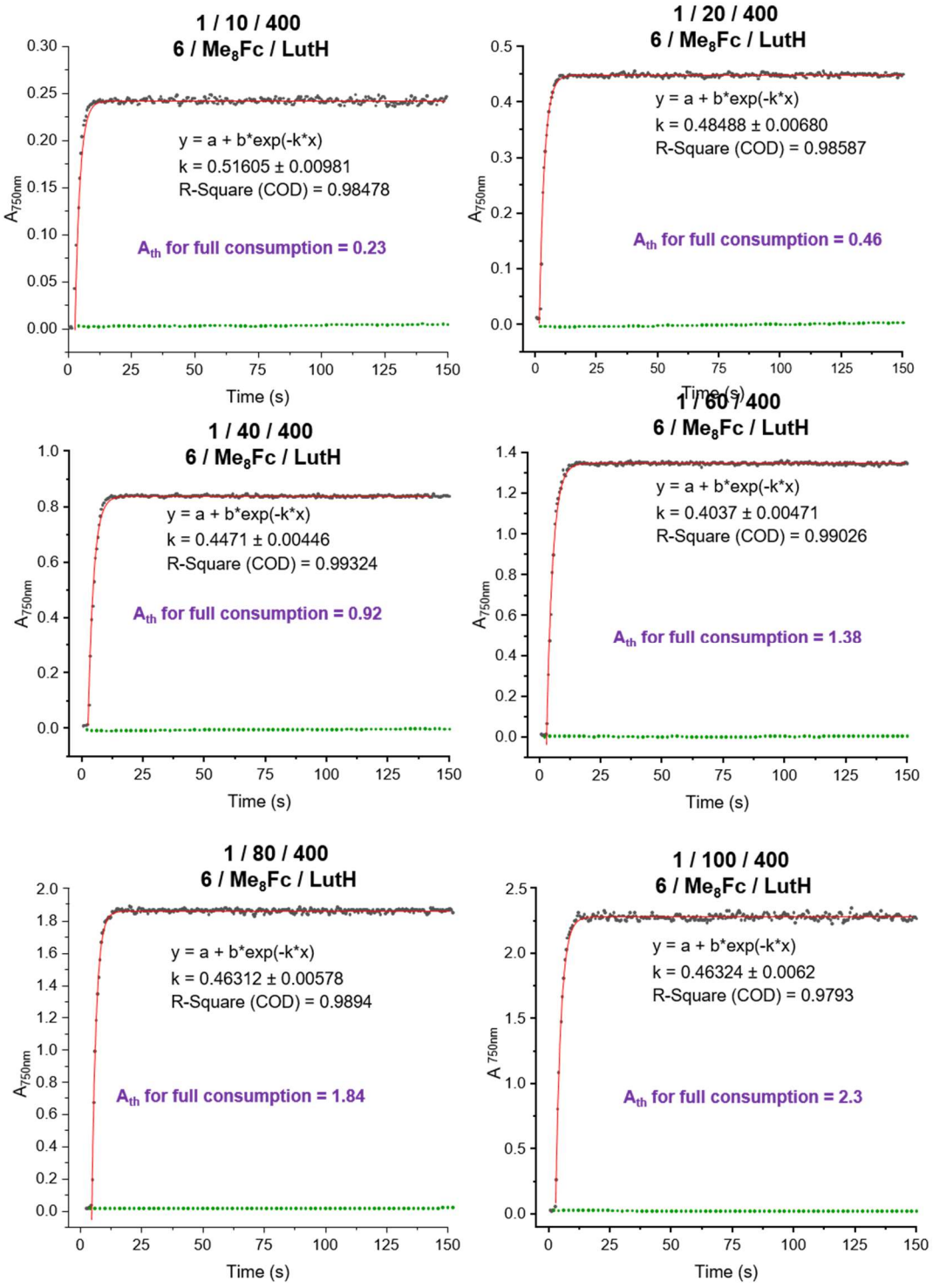

Figure S12. Kinetic profiles (Abs_{max}^{750nm}) for the catalytic ORR by **6** (1 molar eq.) / $LutHBF_4$ (400 molar eq.) / Me_8Fc (10, 20, 40, 60, 80 and 100 molar eq.) in air-saturated acetone together with the blank experiments (green dots) performed with commercial $[Cu(CH_3CN)_4](OTf)$. For each dataset, the theoretical absorbance value corresponding for full Me_8Fc consumption is indicated.

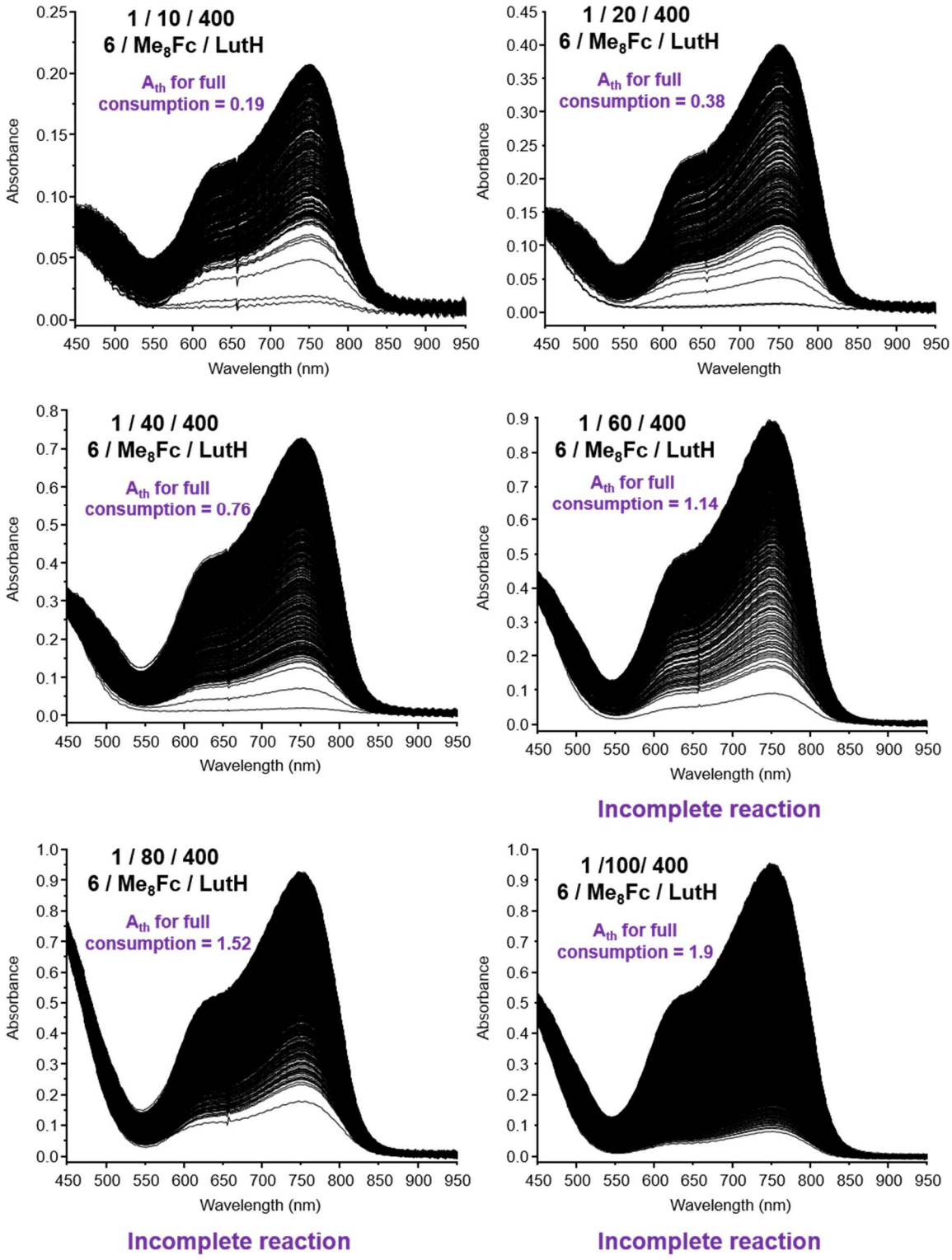

Figure S13. Typical UV-vis changes for the catalytic ORR by **6** (1 molar eq.) / $LutHBF_4$ (400 molar eq.) / Me_8Fc (10, 20, 40, 60, 80 and 100 molar eq.) in air-saturated MeCN. For each dataset, the theoretical absorbance value corresponding for full Me_8Fc consumption is indicated.

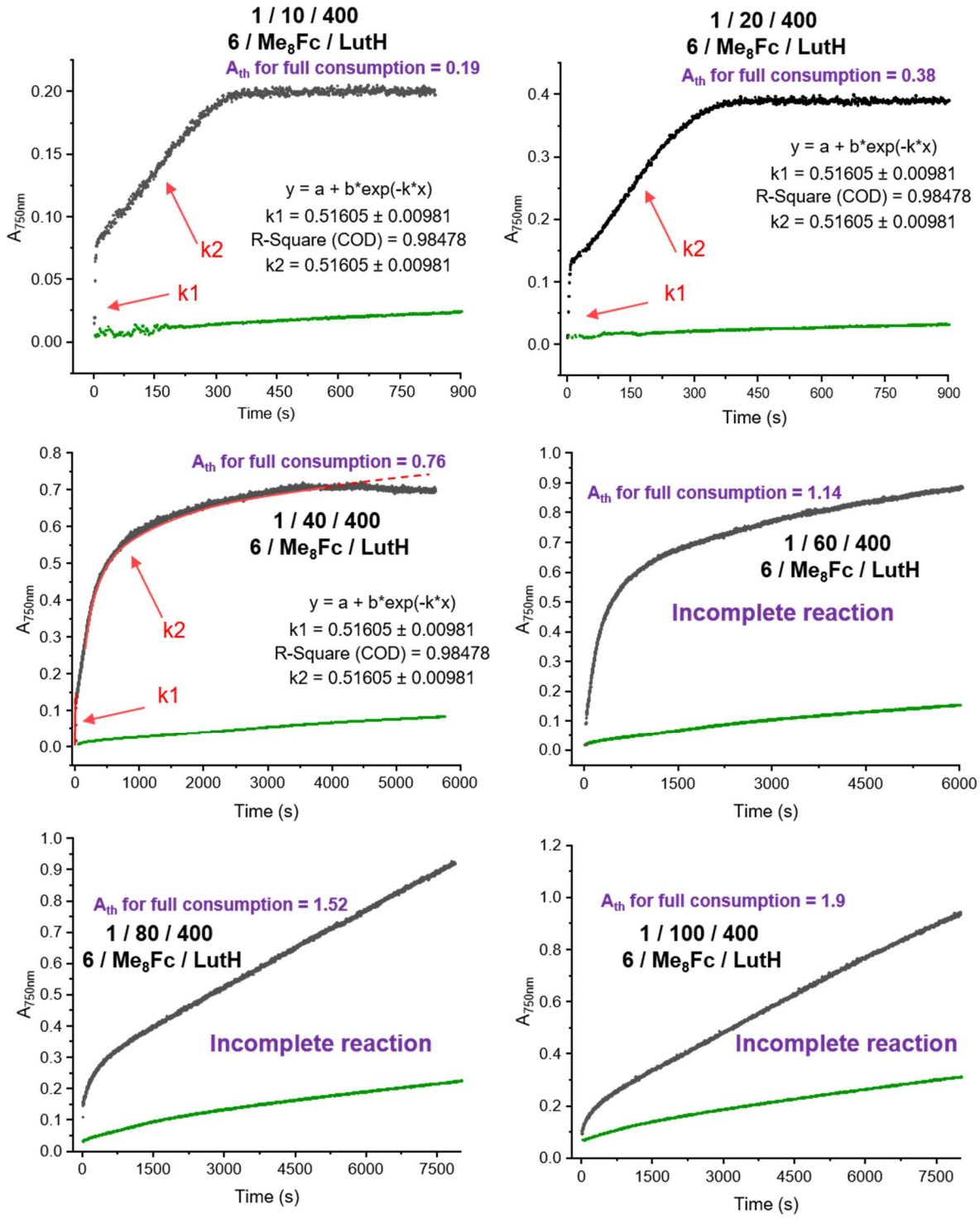

Figure S14. Kinetic profiles (Abs_{max}^{750nm}) for the catalytic ORR by **6** (1 molar eq.) / $LutHBF_4$ (400 molar eq.) / Me_8Fc (10, 20, 40, 60, 80 and 100 molar eq.) in air-saturated MeCN together with the blank experiments (green dots) performed with commercial $[Cu(CH_3CN)_4](OTf)$. For each dataset, the theoretical absorbance value corresponding for full Me_8Fc consumption is indicated.

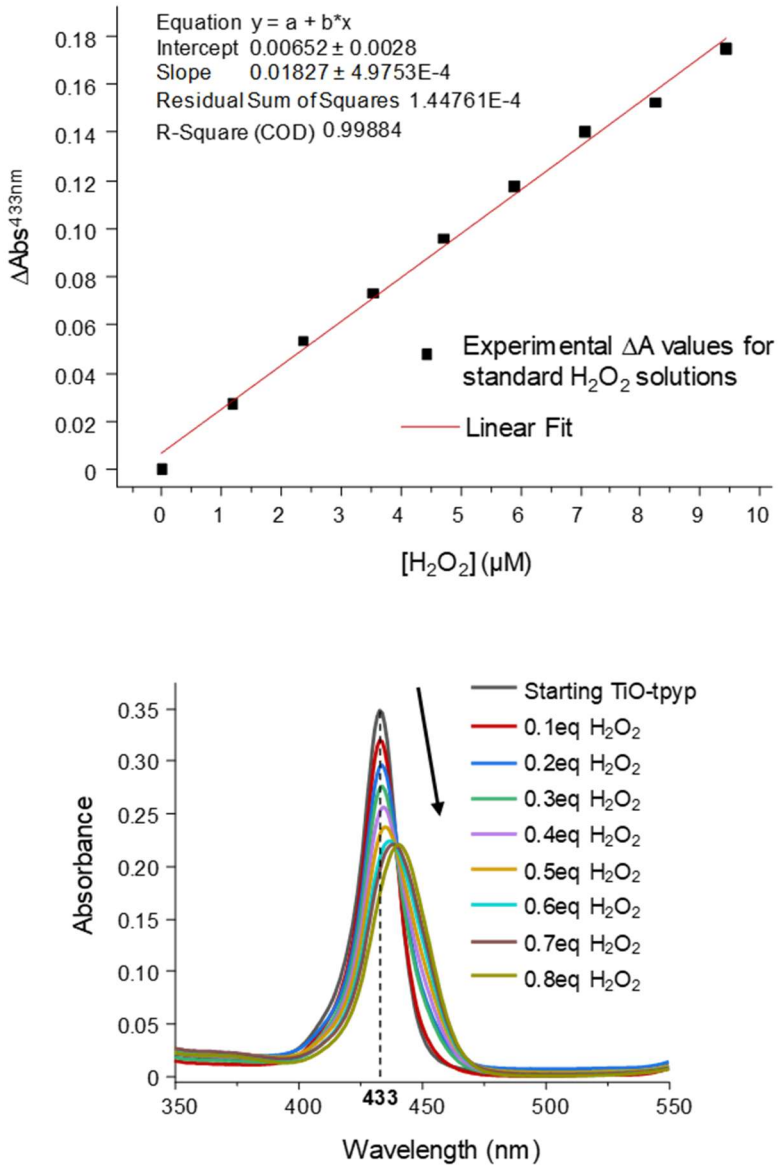

Figure S15. H_2O_2 calibration curve using the TiO-tpyp reagent and corresponding UV-vis traces.

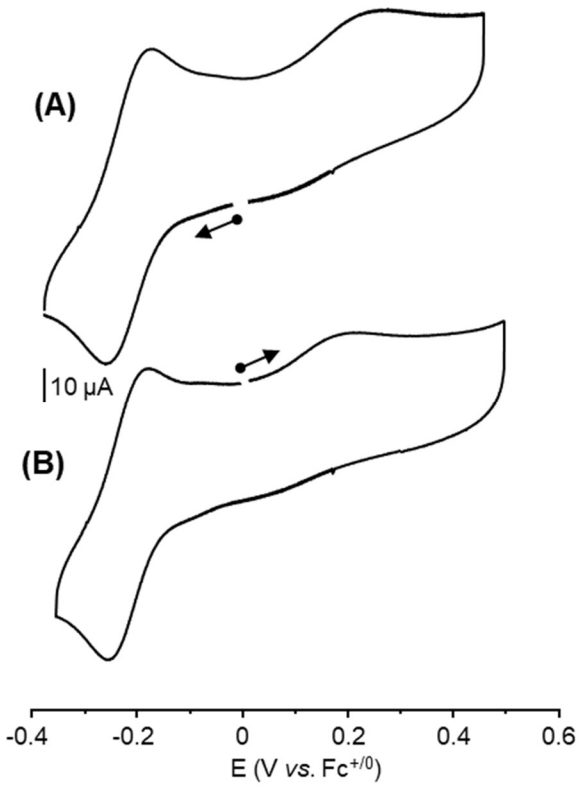

Figure S16. Comparison of the CV curves recorded from the open-circuit potential toward the cathodic (A) and anodic (B) directions. Conditions **6** at 0.6 mM in MeCN + 0.1 M $TBAPF_6$ as supporting electrolyte and glassy carbon as working electrode. The curves corresponds to the initial scan at 100 $mV.s^{-1}$ starting from the open-circuit potential.

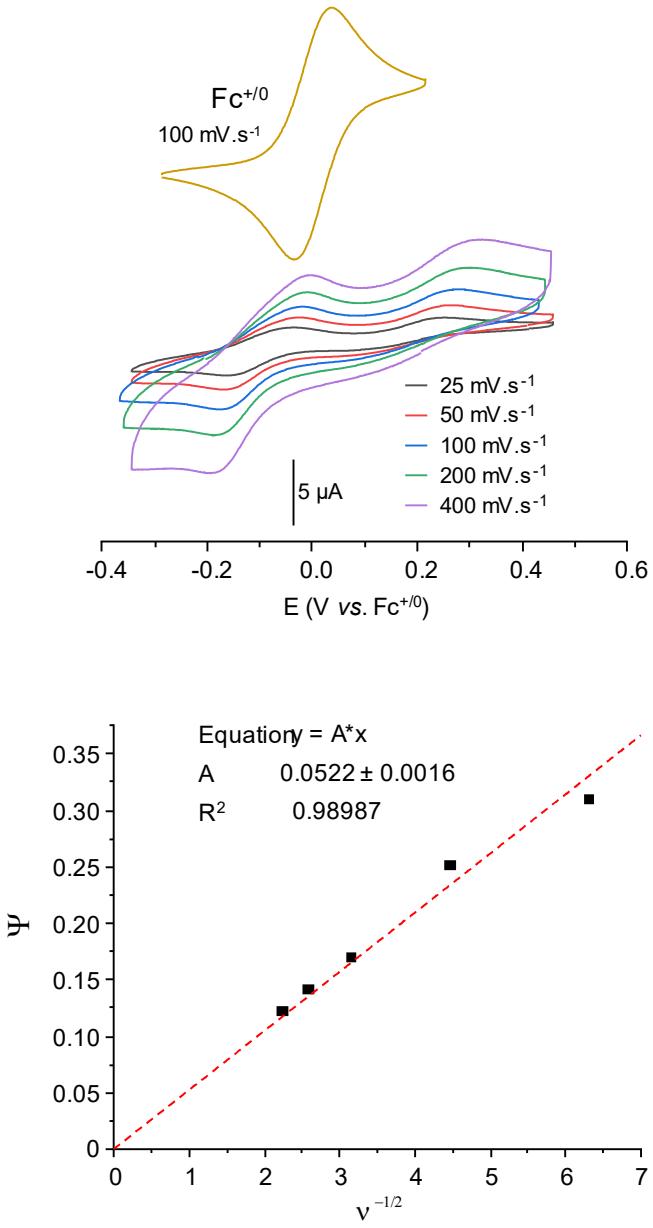

Figure S17. CVs of **6** (0.7 mM) in acetone at different scan rates and experimental plot of Ψ *vs* $v^{-1/2}$ for the redox $Cu^{II}Cu^{I}/Cu^{II}Cu^{II}$ process in **6**.

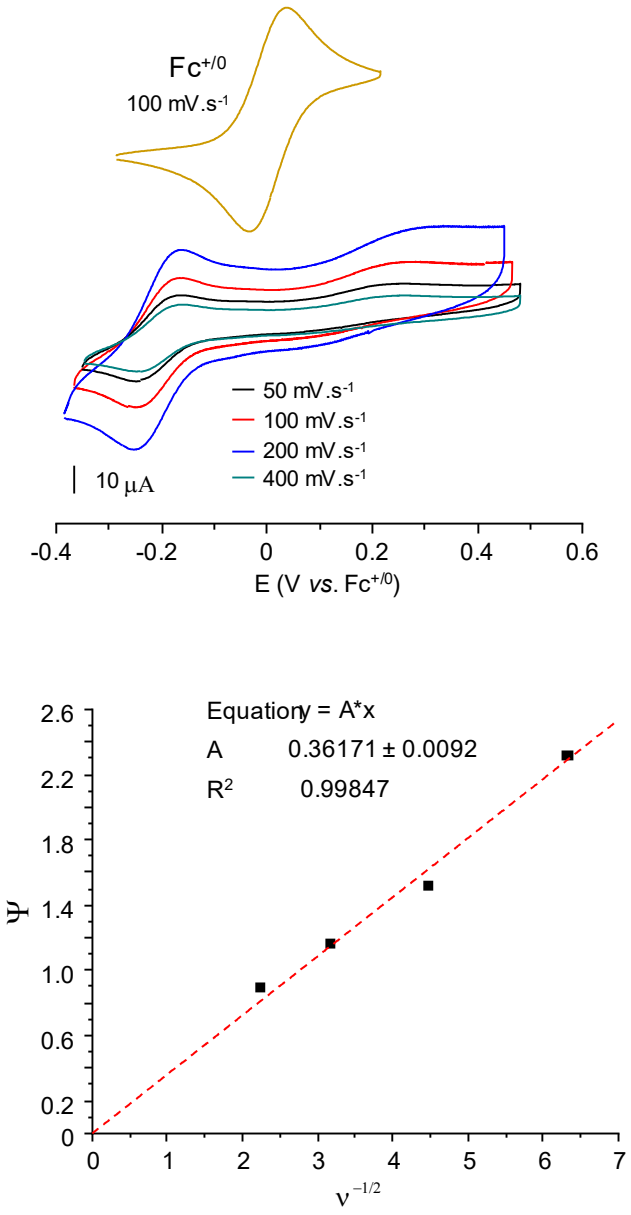

Figure S18. CVs of **6** (0.6 mM) in MeCN at different scan rates and experimental plot of Ψ *vs* $v^{-1/2}$ for the redox $Cu^{II}Cu^{I}/Cu^{II}Cu^{II}$ process in **6**.

Table S1. Crystal data and structure refinement for **6**.

Empirical formula	**$C_{40}H_{41}Cu_2F_6N_4O_7S_3$**
Formula weight	1027.03
Temperature	151(5) K
Wavelength	0.71073 Å
Crystal system	Triclinic
Space group	P_{-1}
Unit cell dimensions	a = 11.0301(4) Å α = 71.825(3)°
	b = 13.4863(5) Å β = 89.191(3)°
	c = 15.6024(5) Å γ = 79.823(3)°
Volume, Z	2168.37(14) $Å^3$, 2
Density (calculated)	1.573 g/cm^3
Absorption coefficient	1.204 mm^{-1}
F(000)	1050
Crystal size	0.284 × 0.244 × 0.142 mm
θ range for data collection	3.756 to 61.012 °
Limiting indices	$-15 \le h \le 11$, $-19 \le k \le 19$, $-22 \le l \le 22$
Reflections collected	26420
Independent reflections	13107 [R_{int} = 0.0362]
Absorption correction	Semi-empirical from equivalents
Max. and min. transmission	0.8995 and 0.7736
Refinement method	Full-matrix least-squares on F^2
Data / Restraints / Parameters	13107/422/786
Goodness-of-fit on F^2	1.026
Final R indices [$I>2\sigma(I)$]	R_1 = 0.0574, wR_2 = 0.1308
R indices (all data)	R_1 = 0.0863, wR_2 = 0.1463

Table S2. Bond length [Å] for **6**.

Cu1	**Cu2**	**2.5475(5)**	C17	C22	1.392(5)
Cu1	S1	2.1798(8)	C18	C19	1.389(5)
Cu1	O1S2	2.176(2)	C19	C20	1.376(6)
Cu1	N1	2.043(2)	C20	C21	1.376(7)
Cu1	N2	1.959(3)	C21	C22	1.392(6)
Cu2	S1	2.1611(8)	C23	C24	1.503(5)
Cu2	N3	2.114(3)	C24	C25	1.384(5)
Cu2	N4	1.945(3)	C25	C26	1.388(5)
S1	C1	1.799(3)	C26	C27	1.381(6)
S2	O1S2	1.450(2)	C27	C28	1.383(5)
S2	O2S2	1.437(3)	C29	C30	1.500(5)
S2	O3S2	1.427(3)	C30	C31	1.388(5)
S2	C2S	1.825(4)	C30	C35	1.387(5)
F1S2	C2S	1.312(5)	C31	C32	1.384(6)
F2S2	C2S	1.317(6)	C32	C33	1.378(7)
F3S2	C2S	1.321(5)	C33	C34	1.376(7)
N1	C8	1.492(4)	S3	O1S3	1.4416
N1	C10	1.484(4)	S3	O2S3	1.4538
N1	C16	1.508(4)	S3	O3S3	1.4330
N2	C11	1.353(4)	S3	C3S	1.8105(12)
N2	C15	1.341(4)	F1S3	C3S	1.3496
N3	C9	1.482(4)	F2S3	C3S	1.3248
N3	C23	1.482(4)	F3S3	C3S	1.3429
N3	C29	1.494(4)	C34	C35	1.391(6)
N4	C24	1.352(4)	S4	O1S4	1.426(9)
N4	C28	1.341(4)	S4	O2S4	1.438(9)
C1	C2	1.399(4)	S4	O3S4	1.417(9)
C1	C6	1.395(4)	S4	C4S	1.791(11)
C2	C3	1.392(4)	F1S4	C4S	1.335(9)
C2	C8	1.507(4)	F2S4	C4S	1.310(8)
C3	C4	1.385(4)	F3S4	C4S	1.327(8)
C4	C5	1.392(4)	S5	O1S5	1.434(8)
C4	C7	1.506(4)	S5	O2S5	1.444(8)
C5	C6	1.396(4)	S5	O3S5	1.424(8)
C6	C9	1.512(4)	S5	C5S	1.801(10)
C10	C11	1.497(4)	F1S5	C5S	1.342(7)
C11	C12	1.380(4)	F2S5	C5S	1.318(7)
C12	C13	1.388(5)	F3S5	C5S	1.335(7)
C13	C14	1.369(6)	O41	C41	1.205(6)
C14	C15	1.380(5)	C41	C42	1.492(7)
C16	C17	1.511(4)	C41	C43	1.498(7)
C17	C18	1.386(5)			

Table S3. Bond angles [deg] for **6.**

S1	Cu1	Cu2	53.72(2)	C11	C12	C13	119.4(3)
O1S2	Cu1	Cu2	99.82(6)	C14	C13	C12	119.2(3)
O1S2	Cu1	S1	100.90(7)	C13	C14	C15	119.3(3)
N1	Cu1	Cu2	139.15(7)	N2	C15	C14	121.9(3)
N1	Cu1	S1	99.32(7)	N1	C16	C17	114.8(3)
N1	Cu1	O1S2	116.63(10)	C18	C17	C16	119.9(3)
N2	Cu1	Cu2	111.60(8)	C18	C17	C22	118.8(3)
N2	Cu1	S1	160.22(9)	C22	C17	C16	121.3(3)
N2	Cu1	O1S2	94.50(10)	C17	C18	C19	120.4(4)
N2	Cu1	N1	84.55(10)	C20	C19	C18	120.4(4)
S1	Cu2	Cu1	54.41(2)	C19	C20	C21	119.9(4)
N3	Cu2	Cu1	140.85(7)	C20	C21	C22	120.1(4)
N3	Cu2	S1	99.66(7)	C17	C22	C21	120.4(4)
N4	Cu2	Cu1	114.01(8)	N3	C23	C24	109.8(3)
N4	Cu2	S1	164.67(8)	N4	C24	C23	115.2(3)
N4	Cu2	N3	84.24(11)	N4	C24	C25	122.2(3)
Cu2	S1	Cu1	71.87(3)	C25	C24	C23	122.6(3)
C1	S1	Cu1	95.54(9)	C24	C25	C26	118.6(4)
C1	S1	Cu2	94.69(10)	C27	C26	C25	119.4(4)
O1S2	S2	C2S	102.13(18)	C26	C27	C28	118.9(4)
O2S2	S2	O1S2	113.91(15)	N4	C28	C27	122.4(4)
O2S2	S2	C2S	104.0(2)	N3	C29	C30	113.2(3)
O3S2	S2	O1S2	114.30(17)	C31	C30	C29	120.2(3)
O3S2	S2	O2S2	116.38(19)	C35	C30	C29	121.4(3)
O3S2	S2	C2S	103.73(19)	C35	C30	C31	118.4(3)
S2	O1S2	Cu1	123.52(15)	C32	C31	C30	120.9(4)
F1S2	C2S	S2	111.4(3)	C33	C32	C31	120.1(5)
F1S2	C2S	F2S2	108.4(4)	C34	C33	C32	119.9(4)
F1S2	C2S	F3S2	107.7(4)	O1S3	S3	O2S3	115.8
F2S2	C2S	S2	111.0(3)	O1S3	S3	C3S	102.7
F2S2	C2S	F3S2	108.1(4)	O2S3	S3	C3S	103.0
F3S2	C2S	S2	110.1(3)	O3S3	S3	O1S3	115.0
C8	N1	Cu1	112.53(17)	O3S3	S3	O2S3	114.9
C8	N1	C16	110.3(2)	O3S3	S3	C3S	102.6
C10	N1	Cu1	102.89(18)	F1S3	C3S	S3	111.8
C10	N1	C8	111.4(2)	F2S3	C3S	S3	111.5
C10	N1	C16	111.8(2)	F2S3	C3S	F1S3	106.3
C16	N1	Cu1	107.63(18)	F2S3	C3S	F3S3	108.7
C11	N2	Cu1	112.0(2)	F3S3	C3S	S3	111.6
C15	N2	Cu1	128.1(2)	F3S3	C3S	F1S3	106.6
C15	N2	C11	119.3(3)	C33	C34	C35	120.0(4)
C9	N3	Cu2	111.36(18)	O1S4	S4	O2S4	115.8
C9	N3	C29	109.5(2)	O1S4	S4	C4S	102.7
C23	N3	Cu2	99.17(19)	O2S4	S4	C4S	103.0
C23	N3	C9	112.6(2)	O3S4	S4	O1S4	115.0
C23	N3	C29	108.7(2)	O3S4	S4	O2S4	114.9
C29	N3	Cu2	115.1(2)	O3S4	S4	C4S	102.7
C24	N4	Cu2	112.2(2)	F1S4	C4S	S4	111.8

C28	N4	Cu2	128.9(3)	F2S4	C4S	S4	111.5
C28	N4	C24	118.5(3)	F2S4	C4S	F1S4	106.3
C2	C1	S1	119.2(2)	F2S4	C4S	F3S4	108.7
C6	C1	S1	120.8(2)	F3S4	C4S	S4	111.7
C6	C1	C2	120.0(3)	F3S4	C4S	F1S4	106.5
C1	C2	C8	121.7(3)	C30	C35	C34	120.7(4)
C3	C2	C1	119.1(3)	O1S5	S5	O2S5	115.8
C3	C2	C8	119.2(3)	O1S5	S5	C5S	102.7
C4	C3	C2	122.1(3)	O2S5	S5	C5S	103.0
C3	C4	C5	117.8(3)	O3S5	S5	O1S5	115.1
C3	C4	C7	121.1(3)	O3S5	S5	O2S5	114.9
C5	C4	C7	121.1(3)	O3S5	S5	C5S	102.6
C4	C5	C6	121.9(3)	F1S5	C5S	S5	111.8
C1	C6	C5	119.1(3)	F2S5	C5S	S5	111.5
C1	C6	C9	122.1(3)	F2S5	C5S	F1S5	106.3
C5	C6	C9	118.7(3)	F2S5	C5S	F3S5	108.7
N1	C8	C2	113.4(2)	F3S5	C5S	S5	111.7
N3	C9	C6	113.9(2)	F3S5	C5S	F1S5	106.5
N1	C10	C11	109.0(2)	O41	C41	C42	121.4(4)
N2	C11	C10	115.3(3)	O41	C41	C43	121.8(5)
N2	C11	C12	120.9(3)	C42	C41	C43	116.8(5)
C12	C11	C10	123.7(3)				

Table S4. NBO analysis of the Cu-Cu bond in mixed-valent Cu^{II}-Cu^{I} species: Comparison of the results obtained for DFT-optimized and X-ray crystal structures of **6** featuring different metal-metal bond lengths.

	Cu-Cu distance (Å)	Wiberg bond index	NBO composition	Occupancy
DFT-optimized	2.719	0.539	43.16% Cu_1 (5.5% 4s, 36.9% 4p, 57.6% 3d) 56.84% Cu_2 (8.0% 4s, 33.3% 4p, 58.7% 3d)	0.748
X-ray	2.5475(5)	0.567	30.54% Cu_1 (4.2% 4s, 34.8% 4p, 61.0% 3d) 69.46% Cu_2 (8.2% 4s, 20.7% 4p, 71.1% 3d)	0.814

Table S5. Mulliken spin population analysis for **6** (DFT-optimized structure).

Center	Cu_1	S	Cu_2	N_1	N_2	N_3	N_4
Spin population	0.274	0.235	0.247	0.083	0.040	0.070	0.038

Table S6. Computed *g*-values and copper hyperfine coupling constants for **6** (DFT-optimized structure).

	g_1	g_2	g_3	g_{iso}
g-tensor	2.045	2.117	2.231	2.131
	A_1	A_2	A_3	A_{iso}
A-tensor (Cu_1)	23.6	74.7	240.2	112.8
A-tensor (Cu_2)	35.2	59.8	229.0	108

Table S7. Theoretical assignments of the main bands of the UV-Vis/NIR spectrum of **6** (DFT-optimized structure).

State	TD-DFT assignement	λ^{calc} (nm)	f^{calc}
1	Core (Cu-S-Cu) → Core (Cu-S-Cus) - IVCT	1255	0.039
2	Metal-Ligand (Cu-thiophenolate) → Core (Cu-S-Cu)	703	0.071
3	Ligand (thiophenolate) → Core (Cu-S-Cu)	481	0.057

Table S8. Theoretical assignments of the main bands of the UV-Vis/NIR spectrum of **6** in the $Cu^{II}Cu^{I}$ form (X-ray crystal structure).

State	TD-DFT assignement	λ^{calc} (nm)	f^{calc}
1	Core (Cu-S-Cu) → Core (Cu-S-Cus) - IVCT	1007	0.038
2	Metal-Ligand (Cu-thiophenolate) → Core (Cu-S-Cu)	613	0.046
3	Ligand (thiophenolate) → Core (Cu-S-Cu)	418	0.034

Table S9. Calculated redox potentials for $Fc^{+/0}$ couple.

G_O^0 (Eh)	G_R^0 (Eh)	$\Delta G_{O/R}^0$(Eh)	E_{Fc}^0 (eV)
-1650.899495	-1651.079309	-0.179813	-4.893

Table S10. Calculated redox potential for the Cu(II)Cu(I)/Cu(I)Cu(I) couple of **6** (DFT-optimized structure).

G_O^0 (Eh)	G_{R-Otf}^0 (Eh)	G_{Otf}^0 (Eh)	$\Delta G_{O/R}^0$ (Eh)	$\Delta G_{O/R}^0$ (V)	$E_{O/R}^0$ (V)
-6215.511418	-5253.678372	-962.009108	-0.176062	-4.791	-0.102

Table S11. ORR experiments performed with **1** and **6** in acetone or MeCN at room temperature using Me_8Fc and $LutHBF_4$ as electron and proton sources. The values obtained for **1** in MeCN (already reported)[32] are listed for comparison.

Entry	[Me_8Fc] (mM)	Cat/e^-/H^+	TON	TON_{max}	k_{obs} (s^{-1})	t (s)	% H_2O_2 Me_8Fc	% H_2O Me_8Fc	TOF (s^{-1})[(b)]
1 in MeCN[32]	0.5	1/10/400	10	10	1.06 ± 0.02	4.1 ± 0.2	90	10	5.3 ± 0.3
	1.0	1/20/400	20	20	0.61 ± 0.02	6.5 ± 0.3	83	17	6.0 ± 0.2.
	2.0	1/40/400	40	40	0.28 ± 0.04	15.0 ± 0.4	57	43	7.6 ± 0.4
	3.0	1/60/400	60	60	0.13 ± 0.01	28.1 ± 0.5	51	49	8.3 ± 0.3
	4.0	1/80/400	80	80	0.15 ± 0.01	32.1 ± 1	38	62	10.7 ± 0.3
	5.0	1/100/400	100	100	0.12 ± 0.01	41.2 ± 2	10	90	14.1± 0.4
1 in acetone	0.5	1/10/400	10	10	0.30 ± 0.05	22.0 ± 0.8	70	30	1.5 ± 0.2
	1.0	1/20/400	20	20	0.13 ± 0.02	44 ± 2	60	40	1.7 ± 0.3
	2.0	1/40/400	40	40	0.08 ± 0.005	55 ± 2	44	36	1.8 ± 0.3
	3.0	1/60/400	60	60	0.05 ± 0.004	91 ± 4	31	69	1.9 ± 0.2
	4.0	1/80/400	80	80	0.13 ± 0.03 0.014 ± 0.006	279 ± 9	23	77	2.3 ± 0.3
	5.0	1/100/400	100	100	0.10 ± 0.02 0.014 ± 0.009	268 ± 10	20	80	2.7 ± 0.4
6 in acetone	0.5	1/10/400	10	10	0.51 ± 0.01	11.2 ± 0.9	42	54	3.1 ± 0.2
	1.0	1/20/400	20	20	0.45 ±0.003	13.4 ± 1.1	25	75	4.4 ± 0.3
	2.0	1/40/400	40	40	0.45 ± 0.004	13.8 ± 1.0	17	83	7.9 ± 0.3
	3.0	1/60/400	60	60	0.40 ± 0.004	15.1 ± 1.2	11	89	10.6 ± 0.4
	4.0	1/80/400	80	80	0.56 ± 0.01	14.2 ± 1.1	12	88	14.0 ± 0.3
	5.0	1/100/400	100	100	0.46 ± 0.006	15.5 ± 1.3	5	95	17.6 ± 0.2
6 in MeCN	0.5	1/10/400	10	10	0.51 ± 0.05 89.9 ± 8	340 ± 30	34	66	< 1
	1.0	1/20/400	20	20	0.58 ± 0.09 122 ± 14	390 ± 35	17	83	< 1
	2.0	1/40/400	40	40	0.55 ± 0.08 178 ± 12	3500 ± 150	10	90	< 1
	3.0	1/60/400	50[(a)]	60	*nd*	> 6000	*nd*	*nd*	< 1
	4.0	1/80/400	40[(a)]	80	*nd*	> 6000	*nd*	*nd*	< 1
	5.0	1/100/400	40[(a)]	100	*nd*	> 6000	*nd*	*nd*	< 1

; [(a)] after 6000 s reaction time; *nd*: not determined; (b) determined for the first kinetic event in the case of multi regimes

Table S12. Crystal data and structure refinement for **II**.

Empirical formula	**$C_{18}H_{14}O_4S_2$**
Formula weight	358.41
Temperature	90(1) K
Wavelength	0.71073 Å
Crystal system	Triclinic
Space group	P_{-1}
Unit cell dimensions	a = 8.0729(3)Å α =96.363(3)°
	b = 9.8805(4) Å β = 104.018(3)°
	c = 11.0153(4) Å γ = 108.327(3)°
Volume, Z	792.37(5) $Å^3$, 2
Density (calculated)	1.502 g/cm^3
Absorption coefficient	0.356 mm^{-1}
F(000)	372
Crystal size	0.422 × 0.263 × 0.059 mm
θ range for data collection	3.892 to 61.014 °
Limiting indices	$-11 \le h \le 11$, $-14 \le k \le 14$, $-15 \le l \le 15$
Reflections collected	19291
Independent reflections	4832 [R_{int} = 0.0222]
Absorption correction	Semi-empirical from equivalents
Refinement method	Full-matrix least-squares on F^2
Data / Restraints / Parameters	4832/0/273
Goodness-of-fit on F^2	1.143
Final R indices [$I>2\sigma(I)$]	R_1 = 0.0317, wR_2 = 0.0809
R indices (all data)	R_1 = 0.0367, wR_2 = 0.0830

Table S13. Bond length [Å] for **II**.

S1	S2	2.0814(5)	C4	C8	1.4993(17)
S1	C1	1.7823(12)	C5	C6	1.3932(17)
S2	C10	1.7826(12)	C6	C9	1.4871(17)
O1	C7	1.2087(16)	C10	C11	1.4062(16)
O2	C9	1.2116(16)	C10	C15	1.4053(16)
O3	C16	1.2059(16)	C11	C12	1.3931(17)
O4	C18	1.2126(15)	C11	C16	1.4894(17)
C1	C2	1.4020(17)	C12	C13	1.3965(17)
C1	C6	1.4094(17)	C13	C14	1.3913(17)
C2	C3	1.3980(16)	C13	C17	1.5020(17)
C2	C7	1.4917(17)	C14	C15	1.3959(17)
C3	C4	1.3891(17)	C15	C18	1.4890(16)
C4	C5	1.3947(17)			

Table S14. Bond angles [deg] for **II**

C1	S1	S2	102.09(4)	O2	C9	C6	123.01(12)
C10	S2	S1	100.68(4)	C11	C10	S2	122.00(9)
C2	C1	S1	119.49(9)	C15	C10	S2	119.06(9)
C2	C1	C6	118.73(11)	C15	C10	C11	118.86(11)
C6	C1	S1	121.78(9)	C10	C11	C16	122.34(11)
C1	C2	C7	122.71(11)	C12	C11	C10	119.74(11)
C3	C2	C1	119.93(11)	C12	C11	C16	117.87(11)
C3	C2	C7	117.36(11)	C11	C12	C13	121.85(11)
C4	C3	C2	121.93(11)	C12	C13	C17	120.66(11)
C3	C4	C5	117.62(11)	C14	C13	C12	117.79(11)
C3	C4	C8	121.47(11)	C14	C13	C17	121.55(11)
C5	C4	C8	120.91(11)	C13	C14	C15	121.69(11)
C6	C5	C4	121.98(11)	C10	C15	C18	122.32(11)
C1	C6	C9	122.18(11)	C14	C15	C10	119.91(11)
C5	C6	C1	119.79(11)	C14	C15	C18	117.77(11)
C5	C6	C9	118.02(11)	O3	C16	C11	123.22(12)
O1	C7	C2	122.54(12)	O4	C18	C15	122.64(12)

Cartesian coordinates from DFT calculations

- Optimized structure for **6** in the Cu(II)-Cu(I) state

Cu	7.69971045523041	12.41635264839144	10.40417239113580
Cu	8.26598707323696	14.64534428687640	11.85417561625451
S	6.84312849375639	13.03159139507239	12.34779425732526
S	6.26767613510856	15.12477420542376	9.04386415405894
F	3.99004228739336	14.89678282573636	10.44052127886137
F	3.72297520599258	14.87887835692900	8.26675021598848
F	4.16696084881968	16.75860748414406	9.30034474114929
O	6.35507230511268	13.64568091910243	9.01531081922571
O	6.87644510590177	15.74510750225988	10.23996248946971
O	6.57782517275902	15.78283283392570	7.77706383973000
C	4.42620640753848	15.43252353213899	9.27902725712576
N	7.58719326478705	10.30200910164237	10.65821629580352
N	9.08875860472532	11.96178545089786	9.05911983939528
N	9.02022425758559	15.05532642614317	13.81415648369261
N	9.96138390360001	15.48506530645068	11.26019589262331
C	7.92352763927349	12.02521140540751	13.37660055660727
C	8.02608680518287	10.63746852023507	13.13306182681098
C	8.86422741195710	9.86486008895028	13.95062759219715
H	8.93162159753626	8.79069788588170	13.75828026843045
C	9.60466509274483	10.41952148833299	15.00018360546163
C	9.47592661263034	11.79669620871569	15.22377619414843
H	10.03060648991914	12.25865091268584	16.04505488953578
C	8.64968929738362	12.61211300665894	14.43863470983508
C	10.51538281275209	9.57417292655609	15.85352964907165
H	10.34161118073760	8.50396836739646	15.68114000748991
H	10.36682998745606	9.78305488592453	16.92296642703819
H	11.57304610382252	9.78392360109147	15.62803178042681
C	7.21425671661483	9.94181099595759	12.06241926045183

H 6.15009744854566 10.20122388830004 12.16856650074390
H 7.30842951521680 8.85269225410548 12.20070728835294
C 8.51012465524438 14.06929556724170 14.81756526208327
H 9.03177752740307 14.23798950449458 15.77607674406424
H 7.44926320976601 14.31395792039490 14.97132980651116
C 8.97157276305562 9.88671420071781 10.32298666330063
H 9.59732133334776 10.09619628387389 11.20551413893969
H 9.04056694095461 8.80477955936597 10.12514125296563
C 9.51392506414892 10.67838439525805 9.15764138259964
C 10.43154810699228 10.14649138322977 8.25134248034125
H 10.74641528988468 9.10734980107257 8.35091910000828
C 10.92558733871004 10.95567235807482 7.22750866998788
H 11.64342197021888 10.55763554066024 6.50927047291544
C 10.47774492505830 12.27439508010320 7.12860906171585
H 10.82933596776342 12.93812397541767 6.33938601914724
C 9.55464965522085 12.73887992080683 8.06073510575354
H 9.16320093354385 13.75481926584623 8.01800162502035
C 6.56796421443681 9.79215503017337 9.66970644313263
H 6.85919742552961 10.18935536294118 8.68733893854623
H 5.61450276362197 10.25962694785985 9.95226071183367
C 6.40726874066719 8.28734696219225 9.58624891478415
C 5.48905475565617 7.61305304721542 10.40868796438405
H 4.87684324579588 8.18034860732554 11.11339766297578
C 5.33558054054227 6.22643209737477 10.32231479795977
H 4.61421623114434 5.71986372177287 10.96603019846380
C 6.09600387239778 5.49147024982950 9.40623995778232
H 5.97365076970484 4.40926244319418 9.33583686996359
C 7.00178439331907 6.15216699045071 8.57031966309655
H 7.58630290946038 5.58841297028975 7.84110534827866
C 7.15203998317547 7.53939885365452 8.65883635364612
H 7.84409681096517 8.05189241371687 7.98639129375055

C 10.47493964388423 14.87511367150898 13.55378929431345

H 11.08100398960173 15.25789227893675 14.39246286057308

H 10.66842637896412 13.79379659035682 13.46994180706818

C 10.87674512626588 15.53947545888660 12.25888784507394

C 12.11904655948320 16.14486290355659 12.07271035204629

H 12.82948413905684 16.18217813308593 12.89894445274060

C 12.42550113287066 16.70101637516029 10.82962920971587

H 13.39147303825512 17.17972809302409 10.66432825926844

C 11.47408677076241 16.64881365304823 9.80920397030528

H 11.66765747188829 17.07979648290290 8.82743219994726

C 10.25036752448705 16.03626322833803 10.06486321787605

H 9.46711886853600 15.98269973744961 9.30893679741067

C 8.79322390708303 16.45796854952461 14.31206875086483

H 9.36192819268428 16.57429432461109 15.25247912903754

H 9.24095667292855 17.12895120284049 13.56521910372431

C 7.34978885494534 16.83586446244992 14.54338221881593

C 6.51966825500754 17.19661499425557 13.47028408539956

H 6.91773172210975 17.18883344562185 12.45299939438805

C 5.19214730526249 17.57339010196968 13.69084120873041

H 4.56018757795230 17.85211255017540 12.84607147370168

C 4.67853031356307 17.60492020297777 14.99213646166968

H 3.64348543574196 17.90466047097276 15.16538567905238

C 5.50002594560552 17.26100378252341 16.07038570280612

H 5.10954760027360 17.29183575978481 17.08909769287273

C 6.82659030490522 16.88084032495212 15.84555694095922

H 7.46795469683108 16.62007305520248 16.69071085924483

- Optimized structure for **6** in the Cu(I)-Cu(I) state without $CF_3SO_3^-$

Cu 7.89101528931459 12.59996309076785 10.64119982102792

Cu 8.50357645109305 14.62492301975742 12.07665476490372

S 6.95356758000546 13.11847651428343 12.57801623680627

N 7.58646586600868 10.35378268321102 10.74990814433701

N 8.99148576563435 12.09803152031541 9.10371083235556

N 9.26312989827636 15.04287859248726 14.17118305254231

N 10.11847332962450 15.63070342467078 11.59155198589932

C 8.09392564562279 12.04333394896801 13.50313296175482

C 8.18489741374540 10.66485550587997 13.18699981765097

C 9.07137321943335 9.85396316895084 13.90944602239193

H 9.12016903998520 8.79005525598988 13.65990523610043

C 9.87617611929437 10.35228352584570 14.94106171652769

C 9.74380353666047 11.70878917912043 15.25625762780728

H 10.33063569649814 12.12444953703321 16.08027089697131

C 8.87028853936819 12.56417616969765 14.56668327467413

C 10.84889661087957 9.46510640485959 15.67555330305883

H 10.45701388828683 8.44382566821987 15.78201003826057

H 11.07270806144377 9.86019284041466 16.67580624621854

H 11.80342354227543 9.39154848392153 15.12930801370534

C 7.29274531725171 9.99840932174022 12.15846927386384

H 6.25092770621195 10.31159784861014 12.33204150039273

H 7.33674778339348 8.90564970050417 12.31260606767944

C 8.74052583077209 13.98659593778863 15.07211468721134

H 9.23404794160154 14.05352160396635 16.06055460811032

H 7.67497452865574 14.22046052414606 15.22224364760419

C 8.91324422540684 9.93978320018769 10.27398603419056

H 9.62498224264060 10.08491053731389 11.10393970499425

H 8.96493059401512 8.87231719099029 9.99381774873820

C 9.37025875726577 10.79339073776460 9.10449013206560

C 10.17592827571218 10.27411668498793 8.08973327853366

H 10.45468905431713 9.21995775623517 8.11530568076853

C 10.60523488866015 11.10671657149224 7.05594941755784

H 11.23334301104044 10.71391953965124 6.25536794592806

C 10.20865101010576 12.44570814909822 7.05859825978924

H 10.51222916034042 13.13218194081661 6.26870004235030

C	9.40368063827541	12.90139140874489	8.09770759982670
H	9.06947588604532	13.93766777836674	8.14385971526491
C	6.47842393583761	9.96011309787618	9.82975811120427
H	6.71925031854226	10.37571947858973	8.83997699846823
H	5.57614573934703	10.47312630481995	10.19517924777425
C	6.21120514724499	8.47187997383236	9.70227016591717
C	5.31597537414834	7.82175313859757	10.56893104784758
H	4.78597513356812	8.40158263469986	11.32809968998544
C	5.08256566279068	6.44760703030559	10.46046441769685
H	4.38016645273306	5.96114900473377	11.13998653902792
C	5.73944741262951	5.69920310934066	9.47734541437670
H	5.55525080630229	4.62698422826962	9.38971538137954
C	6.62184941793239	6.33536600815259	8.59811879857425
H	7.12623125223482	5.76177005199005	7.81820264528164
C	6.85147610650081	7.71043303997369	8.70943880002225
H	7.52394961304210	8.20536269407223	8.00456205782663
C	10.69810702080772	14.91107022759623	13.85848412240881
H	11.34647136752920	15.25758544311013	14.68488811560602
H	10.91436091387870	13.84169735231407	13.70046293652652
C	11.04266833853032	15.66315969789858	12.58692652730699
C	12.25791753568566	16.32974876756509	12.42635496852224
H	12.97300665364681	16.34511695610083	13.24977072697934
C	12.53491274665938	16.97382886241358	11.21960830579833
H	13.47918517403415	17.50161177524962	11.07990870447282
C	11.58008699293292	16.93967160462334	10.20146261208953
H	11.74896007953188	17.43339859636615	9.24478958195659
C	10.38706806369942	16.25887109147039	10.42621077863144
H	9.61244069440707	16.20384730178035	9.66141389422708
C	9.00152012469766	16.39241820456901	14.74644008373196
H	9.45941185093766	16.45546871041522	15.75313759525905
H	9.52416737229005	17.11770851609558	14.10460737688822

C	7.53815090247030	16.76373244218876	14.82775726490216
C	6.81348544312634	17.07289838521027	13.66486764518931
H	7.31445505933329	17.03262210085683	12.69317499594590
C	5.46632606749741	17.43572337365620	13.73746994855767
H	4.91780342748637	17.67513435005628	12.82456810778950
C	4.82363268602727	17.50224164392748	14.97969699903750
H	3.77214735219777	17.78913521428908	15.03764232501378
C	5.53709069994185	17.20708063858039	16.14513464799893
H	5.04493078612072	17.26195863952550	17.11786006939371
C	6.88560944667049	16.84136604155491	16.06676623946319
H	7.44172948184287	16.61493930053180	16.97969477305617

- Optimized structure for $CF_3SO_3^-$

S	5.53252468385583	14.74213967093031	8.76550065995040
F	3.21135484747413	13.90192821137391	7.69744833284823
F	4.87529194084137	13.97673903705700	6.27461662052024
F	3.90276374650052	15.82997345237664	6.92140966665604
O	5.84126996999772	13.33791363410357	9.07116630688613
O	4.75962469275274	15.44907075050451	9.79641307418497
O	6.64081030100358	15.51096296090092	8.18151918344603
C	4.31505081757410	14.60559528275311	7.33903315550796

References.

1. S. Torelli, M. Orio, J. Pécaut, H. Jamet, L. Le Pape and S. Ménage, *Angew. Chem. Int. Ed.*, 2010, **49**, 8249-8252.
2. M. Roemer, B. W. Skelton, M. J. Piggott and G. A. Koutsantonis, *Dalton Trans.*, 2016, **45**, 18817-18821.
3. H. Ohmori, T. Takanami, H. Shimada and M. Masui, *Chem. Pharm. Bull.*, 1987, **35**, 2558-2560.
4. C. L. Ford, Y. J. Park, E. M. Matson, Z. Gordon and A. R. Fout, *Science*, 2016, **354**, 741-743.
5. S. Stoll and A. Schweiger, *Journal of magnetic resonance (San Diego, Calif. : 1997)*, 2006, **178**, 42-55.
6. R. S. Nicholson, *Anal. Chem.*, 1965, **37**, 1351-1355.
7. I. Lavagnini, R. Antiochia and F. Magno, *Electroanalysis*, 2004, **16**, 505-506.
8. M. J. Weaver, *The Journal of Physical Chemistry*, 1990, **94**, 8608-8613.
9. F. Neese, *WIREs Computational Molecular Science*, 2018, **8**, e1327.
10. F. Neese, F. Wennmohs, U. Becker and C. Riplinger, *The Journal of Chemical Physics*, 2020, **152**.

11. A. D. Becke, *Physical Review A*, 1988, **38**, 3098-3100.
12. J. P. Perdew, *Physical Review B*, 1986, **33**, 8822-8824.
13. F. Weigend and R. Ahlrichs, *Phys. Chem. Chem. Phys.*, 2005, **7**, 3297-3305.
14. V. Barone and M. Cossi, *J. Phys. Chem. A*, 1998, **102**, 1995-2001.
15. A. Barrozo and M. Orio, *ChemSusChem*, 2019, **12**, 4905-4915.
16. M. J. Frisch, G. W. Trucks, H. B. Schlegel, G. E. Scuseria, M. A. Robb, J. R. Cheeseman, G. Scalmani, V. Barone, G. A. Petersson, H. Nakatsuji, X. Li, M. Caricato, A. V. Marenich, J. Bloino, B. G. Janesko, R. Gomperts, B. Mennucci, H. P. Hratchian, J. V. Ortiz, A. F. Izmaylov, J. L. Sonnenberg, Williams, F. Ding, F. Lipparini, F. Egidi, J. Goings, B. Peng, A. Petrone, T. Henderson, D. Ranasinghe, V. G. Zakrzewski, J. Gao, N. Rega, G. Zheng, W. Liang, M. Hada, M. Ehara, K. Toyota, R. Fukuda, J. Hasegawa, M. Ishida, T. Nakajima, Y. Honda, O. Kitao, H. Nakai, T. Vreven, K. Throssell, J. A. Montgomery Jr., J. E. Peralta, F. Ogliaro, M. J. Bearpark, J. J. Heyd, E. N. Brothers, K. N. Kudin, V. N. Staroverov, T. A. Keith, R. Kobayashi, J. Normand, K. Raghavachari, A. P. Rendell, J. C. Burant, S. S. Iyengar, J. Tomasi, M. Cossi, J. M. Millam, M. Klene, C. Adamo, R. Cammi, J. W. Ochterski, R. L. Martin, K. Morokuma, O. Farkas, J. B. Foresman and D. J. Fox, *Journal*, 2016.
17. A. E. Reed, L. A. Curtiss and F. Weinhold, *Chem. Rev.*, 1988, **88**, 899-926.
18. K. B. Wiberg, *Tetrahedron*, 1968, **24**, 1083-1096.
19. A. D. Becke, *The Journal of Chemical Physics*, 1993, **98**, 5648-5652.
20. C. Lee, W. Yang and R. G. Parr, *Physical review. B, Condensed matter*, 1988, **37**, 785-789.
21. J. P. Perdew and Y. Wang, *Physical Review B*, 1992, **45**, 13244-13249.
22. M. Drosou, C. A. Mitsopoulou, M. Orio and D. A. Pantazis, *Magnetochemistry*, 2022, **8**, 36.
23. R. J. Gómez-Piñeiro, D. A. Pantazis and M. Orio, *ChemPhysChem*, 2020, **21**, 2667-2679.
24. T. Yanai, D. P. Tew and N. C. Handy, *Chem. Phys. Lett.*, 2004, **393**, 51-57.
25. M. E. CASIDA, in *Recent Advances in Density Functional Methods*, DOI: 10.1142/9789812830586_0005, pp. 155-192.
26. S. Hirata and M. Head-Gordon, *Chem. Phys. Lett.*, 1999, **302**, 375-382.
27. S. Hirata and M. Head-Gordon, *Chem. Phys. Lett.*, 1999, **314**, 291-299.
28. R. E. Stratmann, G. E. Scuseria and M. J. Frisch, *The Journal of Chemical Physics*, 1998, **109**, 8218-8224.
29. F. Neese, *The Journal of Chemical Physics*, 2001, **115**, 11080-11096.
30. N. V. Klassen, D. Marchington and H. C. E. McGowan, *Anal. Chem.*, 1994, **66**, 2921-2925.
31. C. Matsubara, N. Kawamoto and K. Takamura, *Analyst*, 1992, **117**, 1781-1784.
32. J. Mangue, C. Gondre, J. Pécaut, C. Duboc, S. Ménage and S. Torelli, *Chem. Commun.*, 2020, **56**, 9636-9639.